USING EMBEDDED POLYVINYLIDENE FILM SENSORS AND METAL FOIL STRAIN GAGES TO MONITOR THE RESIN CURING PROCESS IN THICK FIBERGLASS-RESIN COMPOSITE LAMINATES

by

Jason Andrew Mills

A thesis submitted in partial fulfillment
of the requirements for the degree

of

Master of Science

in

Mechanical Engineering

MONTANA STATE UNIVERSITY
Bozeman, Montana

November 2013

APPROVAL

of a thesis submitted by

Jason Andrew Mills

This thesis has been read by each member of the thesis committee and has been found to satisfactory regarding content, English usage, format, citation, bibliographic style, and consistency and is ready for submission to The Graduate School

Dr. Douglas S. Cairns

Approved for the Department of Mechanical and Industrial Engineering

Dr. Christopher H.M. Jenkins

Approved for The Graduate School

Dr. Ronald W. Larsen

STATEMENT OF PERMISSION TO USE

In presenting this thesis in partial fulfillment of the requirements for a master's degree at Montana State University, I agree that the Library of said university shall make it available to borrowers under rules of the Library.

If I have indicated my intention to copyright this thesis by including a copyright notice page, copying is allowable only for scholarly purposes, consistent with "fair use" as prescribed in the U.S. Copyright Law. Requests for permission for extended quotation from or reproduction of this thesis in whole or in parts may be granted only by the copyright holder.

Jason Andrew Mills

November 2013

ACKNOWLEDGEMENTS

Thanks are due to the staff in the Mechanical and Industrial Engineering Department at Montana State University. All of the course materials were superbly presented, and any issues or questions raised by the research being performed were excellently fielded by the instructors, many of whom were not directly involved in this research.

Specifically, I would like to thank Dr. Douglas Cairns for his patience and guidance as I worked through this process. Also, Dr. Christopher Jenkins offered encouragement and valuable insight along the way.

None of this work would have been possible without the monetary aid of Sandia National Laboratories and Josh Paquette.

I owe much of my knowledge of manufacturing processes to many of the other graduate students with whom I worked. Ed Meehan provided valuable motivation and data acquisition skills. He and I worked side by side on most of the work presented here. Also, Patrick Flaherty and Tiok Agastra were instrumental in teaching us how to make plates.

And thanks to all my friends and family who supported me in my studies.

-Jason Mills

TABLE OF CONTENTS

TABLE OF CONTENTS - CONTINUED

TABLE OF CONTENTS - CONTINUED

LIST OF TABLES

Table Page

LIST OF FIGURES

Figure Page

LIST OF FIGURES - CONTINUED

Figure Page

LIST OF FIGURES - CONTINUED

Figure Page

LIST OF EQUATIONS

Equation Page

ABSTRACT

The composite manufacturing process is a complex one, with many factors affecting the integrity of the finished components. Most current composite laminate manufacturing processes involve injecting liquid matrix into the fiber laminates. The matrix material then undergoes a curing process, which can create residual stresses and strains.

In order quantify these effects, a method of embedding strain gages into the laminate was developed. Metal foil strain gages (MFSGs) and polyvinylidene film (PVDF) sensors were characterized and embedded into the composite laminate. These sensor circuits were designed to compensate for the temperature fluctuations seen during the cure process, and placed so that they could be used for structural health monitoring purposes after the cure process.

To facilitate this, a double bagging technique was developed for extracting the sensor wires from the mold that allowed for easy egress of the wires, and enabled lead wire access.

PVDF sensors were investigated for usefulness in cure and health monitoring applications. It was determined that, when used with simple charge amplifier circuits, the charge decay of the circuits prevented useful long-term results from being obtained; however, they show promise as shock-loading, short-term sensors.

The composite laminate strains were monitored throughout the cure process, and the MFSGs indicated that residual strains were apparent in the laminate as a result of the matrix cure.

INTRODUCTION

Energy. One of the most common buzzwords associated with modern technology, politics, and even war. Energy is crucial to development and progress. Energy drives the production and distribution of goods and services that makes civilized culture possible. In early times, this energy was primarily personal, using the human body as an engine. Eventually, horses and cattle, much stronger than humans, were utilized. Then came the Greeks with their water power (1), windmill (2), and steam turbine. This was followed by the industrial revolution, and the use of hydrocarbons as an energy source.

As the vast yet finite resources of coal, oil, and gas begin to dry up and deplete, it becomes ever more necessary for civilization to develop methods of producing energy which are sustainable. As industrialism marches onward, it is also becoming readily apparent that these traditional methods of developing energy are permanently scarring the planet that mankind calls home, earth.

It is for these reasons that we have turned to various alternative methods to produce the energy needed to power our homes, offices and factories. One of the most abundant sources of renewable energy is wind energy. Winds blow unimpeded across vast areas of sea and land. The massive energy contained within the wind may easily be harnessed, with little to no damage to our mother planet. And there is no end to the vastness of the resource.

In order to deal with the large scale of the modern wind energy productions, alternative engineering methods and designs must be implemented, and progress must

continue to be made in engineering materials. This work was performed for the advancement of composite materials manufacturing.

Motivation

Primarily, this research is driven by a desire to better understand the behavior of the materials under manufacturing conditions, and to design better components by applying the results of this information back into the design. The specific application is wind turbine blades.

As mentioned previously, wind has been being harnessed as an energy source since the first century AD (2). As the need for more power to drive bigger machines progressed, windmills became larger and more sophisticated. For most of their life, windmills have supplied direct mechanical power to accomplish work as shown by the simple pumping windmill in figure 1.

Figure 1: Windmill for pumping water (terraspirit.com)

As electricity came into common use as an energy source, the first wind turbines were designed to produce electricity in the late 19th century (3). Early wind turbines were small (5-10 kW) and localized. They were often used by rural farm families to provide power to run electric lights and radios. Wind turbines quickly grew in size and scale. They have increased in capacity to 7.5MW behemoths (4) such as the one in figure 2.

Figure 2: Enercon E126 7.5MW wind turbine (windpowermonthly.com)

Installations have grown in massive scales as well. From small, local single turbines have sprung wind farms of hundreds of turbines, the largest of which is capable of producing over 1.3 GW of electricity (5)! Figure 3 shows one such farm near the Montana State University campus in Montana.

As more and more ideal space for these wind farms is utilized, it becomes clear that higher output turbines must be developed, in order to more effectively utilize the space. Turbine output is directly related to turbine size.

Figure 3: Judith Gap, MT Wind Farm (invenergyllc.com)

Thus, the composite blades used in wind turbines will need to become longer, thicker and stronger. The turbines such as those at Judith Gap Wind Farm are standard 1.5MW generators, with blade lengths of approximately 40 meters (6). Not only are the blades themselves large and heavy, but they also become part of a rotating mass, subject to strong wind shock loading and large centripetal forces. The blades must be light, strong, and tough.

With an increase in composite thickness comes a unique problem. Under the current blade manufacturing methods, the resin that is injected into the fiberglass layers generates a considerable amount of heat as it cures, as a result of it being a thermoset polymer. When a thermoset polymer sets, it mechanically shrinks due to the crosslinking of polymer chains (referred to here as thermochemical shrinkage). In thick composite laminates (here defined as being thick enough to have significant through-thickness properties), the temperature may vary greatly through the thickness of the laminate, causing thermal stresses to form, in addition to compressive strains from the

thermochemical shrinkage of the polymer. In order to monitor these stresses and strains, sensors must be placed within the laminate layers of the composite.

Blade Design

Wind turbine blades are designed with a complex geometry, as seen below in figure 4.

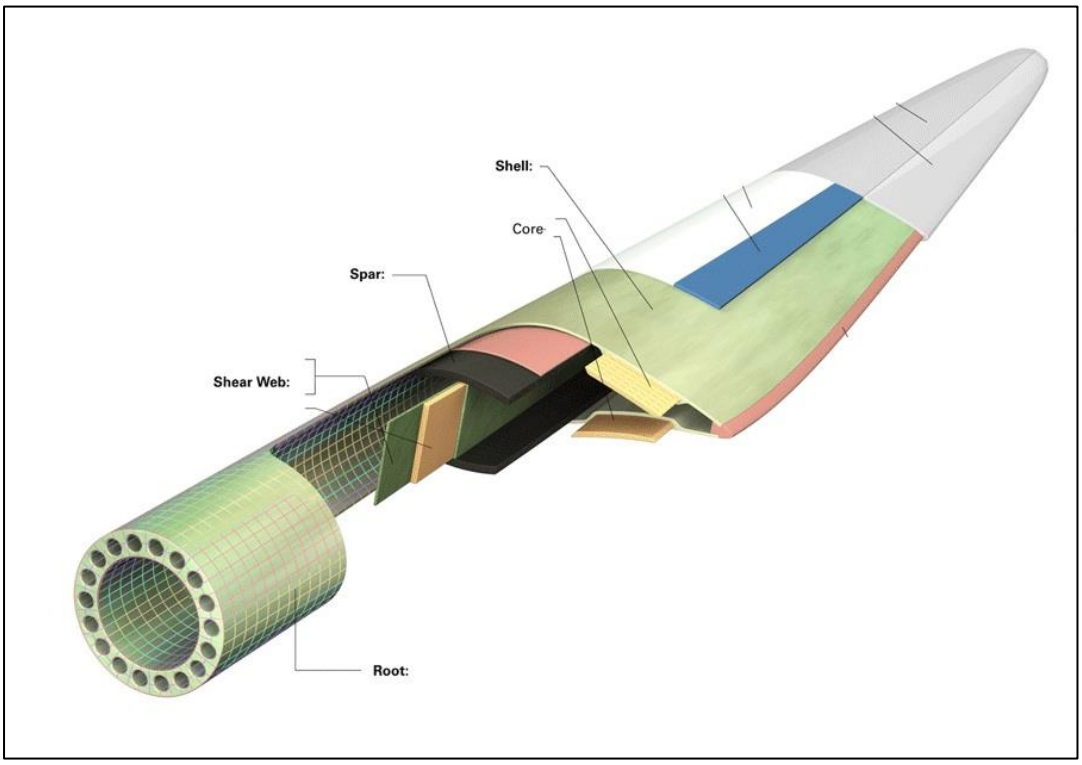

Figure 4: Anatomy of a wind turbine blade (Design News)

Because of this complex geometry, it is difficult to predict and measure the stresses and strains seen by portions of the blade during normal loading conditions. Sensors have previously been placed on the outer shell of the blade, but these are not consistently effective for several reasons. Within a composite laminate, the stresses seen

by each ply may vary greatly, and surface loadings may not be indicative of the actual blade loading. Furthermore, the exterior sensors are subjected to inclement environmental conditions that the blade endures, such as hail and rain, and thus have reliability issues. For these reasons, it is desirable to embed the sensors within the laminate.

Blade Manufacturing

Most wind turbine shells are composed of thick fiberglass-epoxy laminates that are created using a vacuum-assisted resin transfer molding (VARTM) process. This process is described later in Manufacturing Process chapter. The composites are laid up by hand, and visually inspected during the injection and cure process, as seen in figure 5.

Figure 5: Visually inspecting resin injection process (windpowerengineering.com)

This type of visual inspection is not very accurate, as only the outer layer can be seen. Also, the inspector is walking on the blade mold, possibly causing flaws in the composite. This is another reason why sensor embedment is desirable.

Composite Material Failure Modes

Failures in composites generally tend to be catastrophic. In traditional engineering materials, such as steel and aluminum, failure is often indicated by stretching of the material, or cracking. In composites, however, failure tends to be sudden and devastating. The methods of composite failure are given in table1.

Table 1: Composite Failure Methods

Failure	Definition
Fiber Breakage	Physical breakage of the actual fibers
Delamination	Separation between laminate layers
Matrix Cracking	Large cracks in matrix
Matrix Crazing	Micro cracks in matrix
Fiber Debonding	Separation between fibers and matrix

The reasons that these failures are so catastrophic are because the fibers generally tend to be fairly brittle, and as soon as one fiber fails, the mechanical strength of that section is completely reduced by whatever that fiber could carry. Thus when a loading causes one fiber to fail, the load that fiber carried is transferred immediately to the surrounding fibers, and a chain reaction failure occurs.

Composite materials are commonly anisotropic, meaning that they have different mechanical properties in different loading directions. Thus, it is imperative that they laminates be laid up in appropriate directions for the loads being encountered, as the matrix material is significantly weaker than the fibers.

Embedded sensors can be utilized post-cure for health monitoring purposes to test these stresses. They can give an indication of a compromised blade portion before failure occurs, enabling safer, more opportune, and less damaging repairs to be performed. They

can also indicate whether damage is critical, potentially saving money on unnecessary repairs. Another use for the sensors post-cure is to monitor actual stresses on the blades, and allow for better, more efficient blade design.

External blade monitoring is commonly referred to as non-destructive testing (NDT). Current NDT methods are very costly and time-consuming, involving x-ray, sonar, and thermography methods, among others (7). These methods even go as far as to include tower- and blade-climbing robots, such as the one pictured in figure 6.

Figure 6: Tower-climbing NDT robot (Helical Robotics)

With sensor embedment, the loading conditions being endured by the blades could be sent to a laboratory, where a few technicians could monitor entire wind farms. Most of these loadings could even be automatically monitored, perhaps setting an alarm when loadings reached critical levels.

BACKGROUND

Composite Materials

A composite material is formed by combining two or more distinct materials (constituent materials) to create a new material with enhanced properties (8). The constituent materials are divided into two types: matrix and reinforcement. The reinforcement material is what provides the driving mechanical properties of the composite. The matrix material is essentially the medium that holds the reinforcement material in place and acts as the mechanical interface with which to interact with the reinforcement.

Composites exist in various forms in nature, the most common being wood, which is a composite made up of cellulose fibers and lignin (9). The first man-made composites appeared in the form of clay matrix bricks reinforced with straw. Composites are desirable engineering tools for many reasons. They have very good strength-to-weight properties. Composite parts can be manufactured to have distinct mechanical properties in different loading directions, within the same part. Also, complex part geometries are easily manufactured.

Composites in Wind Energy

It is for these reasons that composites use abounds in the burgeoning wind energy field. Specifically, and the in the realm of this project, wind turbine blades are manufactured from composite laminates. Wind turbine blades are comprised of complex, sweeping geometries. The usage of composite laminates aids in ease of manufacture of

these designs. Wind turbines must easily rotate in the wind, and are mounted on gearboxes high above the ground. Thus, they must be able to withstand large wind forces while remaining relatively lightweight. Wind turbine blades are also subjected to severe loading conditions including strong shock loading from wind gusts. This means that they must exhibit unique mechanical properties. The use of composites makes it possible to meet these requirements.

Currently, wind turbine blades made by Sandia are manufactured from fiberglass/epoxy composite laminates. The strong mechanical properties of the glass, combined with the low cost of manufacture make this an ideal choice. In order to design better blades, and to improve manufacturing ease and reliability, it is desirable to investigate interlaminar stresses and strains of the fiberglass composites.

PREVIOUS WORK

Montana State University

Montana State University has been involved with much work in the field of composites research, under the direction of Dr. Douglas Cairns. Specifically, work has been performed in the realm of wind turbine composite research. Much of the work presented here is built upon the research of others. In particular, much useful manufacturing information was gained from the work of Nathan Palmer (10) whose studies involved examining bond strength and mechanical integrity of fiberglass composites with embedded sensors. Palmer performed loading tests on composite coupons with various sensors in various configurations, in order to determine the effects of the sensor on mechanical properties. The sensor essentially acts as a large flaw in the composite material. The manufacturing methods, sensor treatment methods, and observations outlined in that document were utilized in the completion of this work.

Additional information on manufacturing composite laminates with embedded sensors was taken from work performed by John Ehresman in completion of his work (11). Specifically, this work guided sensor type selection and manufacturing methods. The specific PVDF and MFSG sensors used were determined to be practical for this work in Ehresman's studies.

Additional insight on embedded sensor types and strategies for successful laminate construction was taken from the work of J.C. Blockey, in his thesis (12).

As can be determined from these previous works, there is a great deal of interest and utility in developing "smarter" wind turbine blades. The additional control and

monitoring capabilities in these laminates will directly affect quality, cost, and efficiency of wind turbines in positive ways.

Additional Previous Cure Monitoring Research

Because composites are such an important engineering tool today, much research work is being performed in understanding the cure process, and all of the changes and effects that take place as a result of the thermochemical setting of the resin.

Many advances are currently being made in utilizing fiber optics as sensors in composites. These are particularly useful for several reasons:

1. The optical fibers act very similar to the composite fibers, creating negligible effects to the mechanical properties
2. The fiber optic sensors may effectively run the full length of the composite part, giving full-field monitoring of the part. In addition, multiplexing may be used to turn the fiber into multiple gages, each measuring independent loads along the part.
3. The sensors are highly accurate to within +/- 1 microstrain.
4. Fiber optics sensors may be used to measure both strain and temperature (13).

The most common type of fiber optic sensor used for this testing is the Fiber-Bragg grating sensor. Essentially, the grating is a section of the fiber that transmits all light wavelengths but one, and reflects that wavelength back (14). As the grating is strained, the refractive index changes, and different wavelengths are transmitted back, allowing the strain to be measured. The very work of monitoring composite cure with fiber optics is being actively pursued by several large institutions including NASA (15),

the Harbin Institute of Technology (16) and the Korea Advanced Institute of Science and Technology (17).

Why Not Optics?

As good as the fiber optic sensors are in the realm of composites cure monitoring, they still pose some major problems: the equipment used to monitor them is prohibitively expensive for large scale use, and is very complex. Additionally, the fiber egress and interface portions of the design are difficult to master, due in part to the brittle nature of the fibers, and much research has been done specifically to design a useful interface (18), (19), and others.

Equipment and design breakthroughs will be necessary in order to effectively use fiber optic sensors, and MFSGs are inexpensive, well characterized, and easy to implement.

Other Previous Cure Monitoring Research

Little previous work has been done on the actual monitoring of physical stresses and strains of composites during the cure process. There does exist some previous research on this topic, which was referenced in analyzing this research. This includes strain monitoring work with thermoplastic resins (20) and residual strain monitoring work (21).

Other Sensors

Very little information is actually available on composite laminate cure mechanical processes. In order to provide current manufacturers with ready, affordable

solutions to track residual production strains and perform in-field health monitoring, this project to use inexpensive, proven sensors was designed.

Additionally, there has been little work with the use of PVDF sensors in composite laminates to measure temperature and strains. A major portion of this work went into exploring and characterizing this application of these sensors.

SENSORS AND CIRCUITS

Introduction

This section will introduce the different types of sensors utilized within the laminates that were tested, and the accompanying circuits and data-logging that goes along with them. Sensors were selected based on criteria of cost, technical specifications, and ease of use.

Background

The two main types of strain gages used in completion of this work are metal-foil strain gages (MFSG), and polyvinylidene fluoride (PVDF) film piezoelectric sensors. These sensors were selected based on several factors.

The first consideration is cost. Both of these sensors types are fairly common and produced in large numbers. MFSG's are a staple of engineering strain sensing, and are very well understood. PVDF's have recently come into common usage, and are readily available. More importantly, the equipment costs for harnessing the data from these sensors is minimal. Some other sensor methods that were investigated in the aforementioned works, such as Fiber-Bragg grating with fiber optics, are very expensive to employ, and the equipment required to successfully utilize them is currently prohibitively expensive.

Additionally, these sensors have been investigated for structural integrity when inserted into composite laminae, and have been shown to maintain good mechanical

properties of the laminate when properly treated (10). This is an important consideration when dealing with the large scale of wind turbine blades.

Finally, these sensors fit within the specifications required for the conditions that would be encountered in the curing and testing processes. An important consideration of inserting these sensors into the laminates to observe cure stresses was also the ability to later utilize the sensors in health monitoring of composite structures upon installation. All work was performed with this goal in mind. Table 2 shows the exact sensor types that were used.

Table 2: Sensors utilized in testing

Sensor Specifications		
Type	Manufacturer	Model
MFSG	Omega	KFG-5-120-C1-11L1M2R
MFSG	Omega	KFG-5-120-C1-11L3M3R
PVDF	Measurement Specialties	LDT1-028K
PVDF	Measurement Specialties	LDT4-028K
Thermocouple	Omega	GGJ-24

Metal Foil Strain Gages (MFSGs)

One of the main sensor types utilized in this work was the metal foil strain gage. MFSGs have been in use since the 1930s. They are a staple of engineering stress measurements. MFSGs are inexpensive, plentiful, and are very well understood. They can be purchased in a variety of configurations. An example like the ones used in this research is shown below in figure 7.

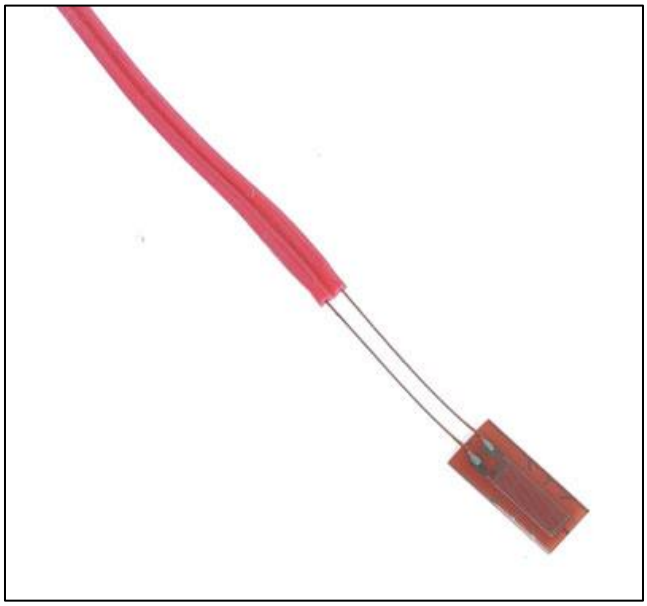

Figure 7: Metal Foil Strain Gage with Lead Wires (Omega.com)

MFSGs consist primarily of a thin metal foil embedded in a flexible, insulating backing. MFSGs rely on the principle of electrical conductance. The strain gage is adhered to the surface of the material to be tested. As the material is strained, the metal foil will strain with it. As the metal foil strains, its geometry changes. With the geometry changes of the metal foil, the resistance through the foil pattern changes as well. The foil pattern can be manufactured such that the resistance change is inversely proportional to the amount that the gage is strained. This proportion is known as the gage factor. Thus strain can be determined from equation 1.

$$\varepsilon = \frac{1}{G_f} * \frac{\Delta R}{R_G}$$

Equation 1: Strain from resistance

In this equation, ε is strain, G_f is the gage factor, ΔR is the change in resistance of the strain gage, and R_G is the initial resistance of the strain gage. MFSGs are manufactured in many different shapes and styles. The ones utilized in this testing were primarily Omega KFG-5-120-C1-11L1M2R gages, as depicted in Figure 7. The specifications for this strain gage are given in table 3.

Table 3: Specifications for MFSG used in this testing

Parameter	Value
Metal Foil Strain Gage, Type	Omega KFG-5-120-C1-11L1M2R
Gage Factor	2.08 +/- 1.0%
Unstrained Resistance (Ω)	120.4 +/- 0.4
Unstrained Length (mm)	5

One of the issues with using MFSGs is that electrical conductivity of metals is adversely affected by temperature. These changes are documented and must be accounted for. The strain gages have been tested and characterized to find a temperature coefficient that is applied to the gage factor. Thus, when performing tests with MFSGs, temperature must be monitored and accounted for in the data analysis, to ensure consistent results.

Another problem that arises in the use of MFSGs, which is related to temperature, is that change in temperature of the lead wires will also affect the resistance of the lead wire. Due to this phenomenon, a variant of the strain gage depicted above was also utilized in this testing. By utilizing two wires on one side of the strain gage, temperature effects are cancelled, and the circuit remains symmetrical. This will be further explained in the circuits section below. The three-wire strain gages utilized were just a three-wire

version of the two-wire gages described above. The specifications for these gages are identical to the two-wire gages previously specified in Table 2.

Polyvinylidene Fluoride Film (PVDF) Sensors

PVDF is a polymer that exhibits strong piezoelectricity. The piezoelectric effect is observed in certain materials when an electrical charge is generated as a result of applied mechanical stress. (22). As a piezoelectric, PVDF can be utilized as a strain gage. When a PVDF is strained, it will create an electric charge that can then be measured and calculated into a strain measurement.

PVDF film sensors are useful in strain measurement due to their relatively high output. Small stresses cause notable electrical charges to be generated. In addition to measuring strain, they are also able to measure impacts well.

The PVDF sensors used in this testing were Measurement Specialties LDT1-028K sensors, identical to the one shown in figure 8.

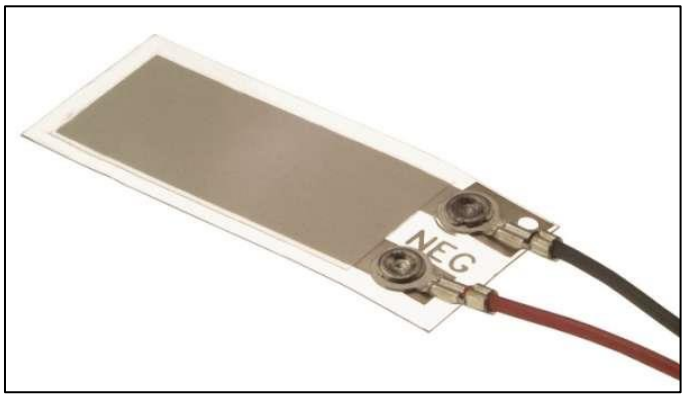

Figure 8: Measurement Specialties LDT1-028K (meas-spec.com)

This particular sensor was chosen due to its relatively small size and its application to a Mylar sheet. This made it easy to adhere into the laminate, and also makes the sensor more useful for measuring bending stress, as the Mylar sheet changes the location of the neutral axis, causing the output of the piezo to be much higher in a bending scenario. Initially, a five inch version of this sensor was utilized in testing, but porosity issues in the resin injection process made the smaller sensor a much better fit. The specifications for this sensor are shown in table 4.

Table 4: PVDF Sensor Specifications

Parameter	Value
PVDF Type	Measurement Specialties LDT1-028K
Piezo Strain Constant (10^{-12} $(C/m^2)/(N/m^2)$	d_{31} : 23; d_{33} : -33
Pyroelectric Coefficient (10^{-6} C/m^2*K)	30
Capacitance (pF/m^2)	380
Temperature Range (deg. C)	-40 to +80

PVDF film sensors were also used due to previous embedment research performed at MSU. More information on actual response of the PVDF films was desired, and the composite laminates provided a good test bed for this type of research.

Thermocouples

A thermocouple is a temperature measurement sensor created by joining two dissimilar metals at one end. When subjected to temperature changes, the junction produces an electrical potential (23). This voltage may be calibrated and measured to find temperature at the junction. Type J thermocouples were utilized in this testing. The

thermocouples were manufactured from type J wire (iron-constantan) using a thermocouple welder. PFA-insulated wire was selected to aid in reduction of air ingress during the manufacturing process. An example of this thermocouple wire may be seen in figure 9.

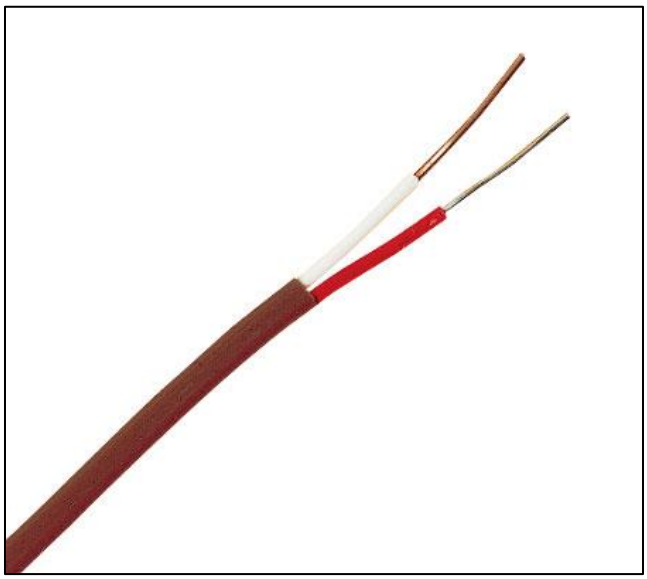

Figure 9: Type J thermocouple wire (omega.com)

Type J thermocouples were selected for several reasons. The wire is low cost and readily available. Type J thermocouples have a limited temperature range, but exhibit high output. Due to the limited temperature range that the composites were subjected to, this made type J a good fit.

The thermocouples were utilized in this experiment to calibrate the strain gages, and as a reference for the portions of the experiment that involved separating temperature effects from strain output of the strain gages.

Circuits

In order to capture useful readings from the various gages utilized, various circuits had to be employed. The circuitry involved was different for the two strain gage types used, as the gages operate on different principles.

Wheatstone Bridge

MFSGs indicate strain by measuring resistance changes of the metal foil. These resistance changes are very small, and are difficult to measure accurately. Resistance of a circuit is determined by using Ohm's Law, equation 2.

$$I = \frac{V}{R}$$

Equation 2: Ohm's Law

Here I is the current of the circuit, V is the voltage differential of the circuit, and R is the resistance of the circuit. If a voltage measurement is to be used to determine the resistance of the circuit, a constant current must flow through the circuit at all times. Equipment to supply a constant current is costly and complex, as the resistance of the strain gage changes constantly under loading. However, constant voltage supplies are relatively inexpensive and when used with a Wheatstone bridge, they allow voltage measurements to be used to determine resistance of a circuit. Furthermore, as will be explained, Wheatstone bridges allow for simple temperature compensations in the circuit.

In a Wheatstone bridge, a source voltage is applied across the strain gage. The voltage difference is measured, and resistance changes in the gage appear as voltage

potential differences. Two variants of the Wheatstone bridge were utilized in this experiment. The first variant, the quarter bridge, is detailed as follows. A schematic is shown in figure 10.

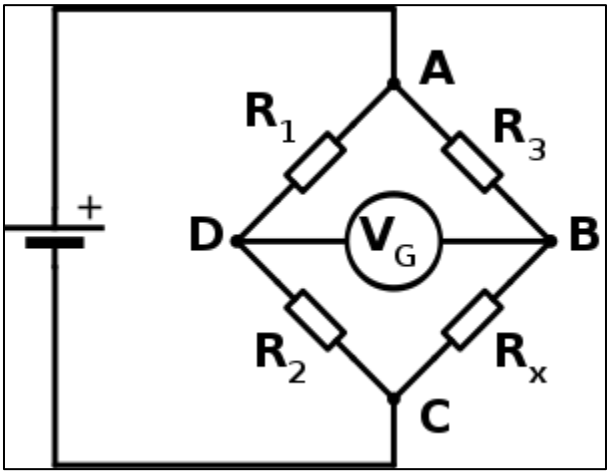

Figure 10: Wheatstone bridge circuit.

In the bridge utilized in this testing, R_x represents the variable resistance of the strain gage. R_1, R_2, and R_3 are fixed resistors that have the same resistance as the unstrained strain gage (in this case 120 ohms). A source voltage is applied across terminals AC, and the voltage is monitored at terminals DB. In an unstrained condition, that is, all resistances are equal, V_{DB} is null. But as R_x changes, a voltage potential will develop at DB. This potential can be determined using Kirchoff's first and second rules. The voltage V_G is then given by equation 3.

$$V_G = \left(\frac{R_x}{R_3 + R_x} - \frac{R_2}{R_1 + R_2}\right)V_s$$

Equation 3: Reference voltage from Wheatstone bridge

Realizing that R_1, R_2, and R_3 are equal, and that V_G is easily measured, R_x can be determined. Once the value of R_x is known, strain can be calculated from equation 1.

As mentioned previously, temperature affects the resistance in the strain gage. In this testing, the laminate underwent temperature changes, and this had to be accounted for. One method of negating temperature effects was to utilize a half-bridge circuit. This circuit is wired identical to the quarter bridge circuit, except that R_3 is replaced by another strain gage, R_y, identical to R_x. This strain gage is placed in the laminate such that it is not subjected to any mechanical strain, but still undergoes the same temperature changes seen by R_x. This, in effect, cancels temperature effects on the resistivity of the strain gage, and only true strain effects are seen in the voltage potential V_G.

If two bridges are used to monitor a sample, with one being a quarter bridge, and one being a half bridge, the temperature may also be determined from the just the strain gages, without any additional temperature monitoring equipment necessary. The strain reading of the quarter bridge can be subtracted from that of the half bridge, and the resulting strain is "thermal" strain that is just a result of heating of the gage. This resulting thermal strain can then be calibrated to determine temperature. This is explained further in the data analysis section, as well as in figures 38-40.

As mentioned previously, temperature changes of the lead wires affect the sensitivity of the strain gage. Copper lead wires increase resistance approximately twenty percent per every hundred degrees Celsius temperature change (24). The three-wire strain gage was used to eliminate this error, and the gage circuit is constructed as shown in figure 11.

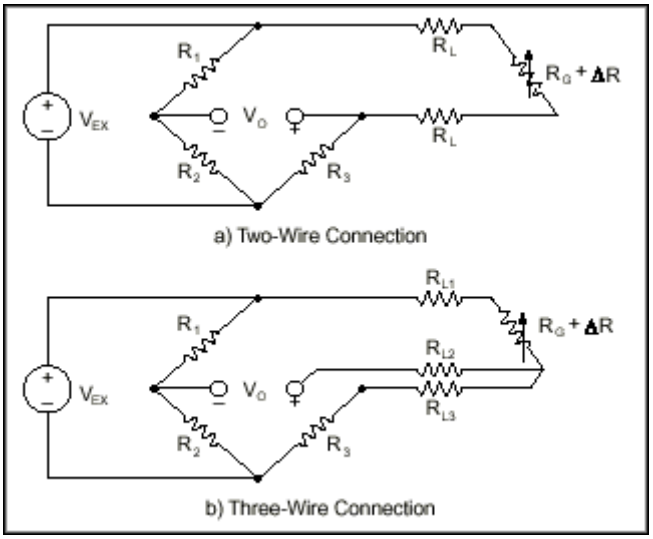

Figure 11: A three wire strain gage circuit (bottom) compared to a two-wire circuit (top)

From figure 11 it can be seen that the bridge is now balanced, as it is symmetrical about the horizontal axis. Any temperature changes in the lead wires, whether due to ambient changes or resistive heating, will be negated. This is an important factor in this project, since the plate undergoes an elevated temperature cure process. Resistance changes to R_{L2} will not matter, since no current is flowing, as it is just a reference wire. Equation 2 still applies to this circuit as well.

The Wheatstone bridge circuits were manufactured on an engineering breadboard using standard 120-ohm resistors. The circuit was powered by a Hewlett Packard 10-volt DC power supply.

PVDF Charge Amplifier Circuit

When PVDFs are strained, they produce a charge. In order to utilize them as sensors, this charge must be converted to a voltage output. So for each PVDF used, a charge amplifier circuit was constructed, as seen in figure 12.

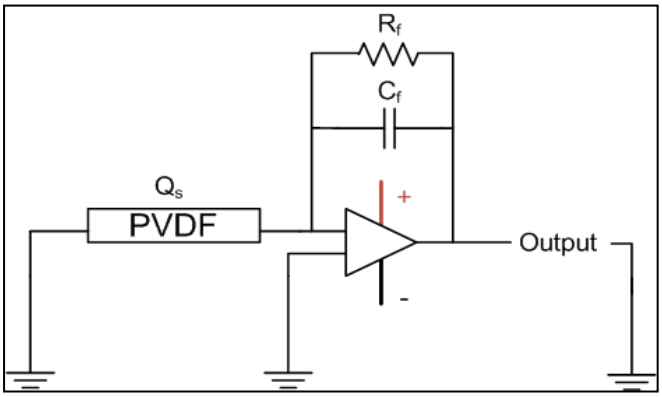

Figure 12: Schematic of a simple PVDF charge amplifier circuit

A charge amplifier is a current integrator circuit, and does not actually amplify a charge. The operation of this circuit is as follows. As a charge is developed in the PVDF, it is transferred to the reference capacitor, C_f. Then the output voltage is proportional to the charge across C_f, and consequently, the PVDF. Essentially, the charge amplifier circuit is a converter from charge to voltage.

The PVDF can then be strained, and the output voltage can be calibrated to represent strain of the PVDF. The op-amp amplifies the voltage signal to a level useful for measurement, and the resistor R_f provides DC stability and governs the lower frequency limit of the circuit (25).

An important consideration of this type of circuit is that it is time-dependent. The charge decays according to the time constant set forth by the RC circuit in the charge amplifier, according to equation 4.

$$\tau = R_f * C_f$$

Equation 4: Time constant of RC circuit

Here τ is the time constant, R_f is the feedback resistor value, and C_f is the capacitance of the feedback capacitor. The time constant is derived from the time-dependent equation for voltage in an RC circuit shown in equation 5.

$$V(t) = V_0 e^{-\frac{t}{RC}}$$

Equation 5: RC circuit voltage function

Here V_0 is the voltage of the circuit at t=0. The time constant τ is defined as the time required for the voltage in the circuit to reach a value of V_0/e. The values of the resistor and capacitor could be varied to increase or decrease the time constant, in order to modify the circuit to useful parameters. As will be seen, the decaying nature of the charge in these circuits reduced the effectiveness of PVDFs for purposes of long-term strain and temperature monitoring.

PVDF Temperature Compensation

Like the metal foil strain gages, PVDFs are subject to temperature effects that affect their output. However, unlike the MFSGs, this is due to pyroelectric effects in the piezo material. When a pyroelectric material such as PVDF is heated, the resulting energy input causes polarization of the crystals in the material, causing a voltage potential to develop across the crystal. This resulting voltage potential creates a charge within the PVDF sensor (26). This charge increase due to temperature may appear as though the PVDF sensor is being strained. In order to compensate for this, a circuit was constructed as shown in figure 13.

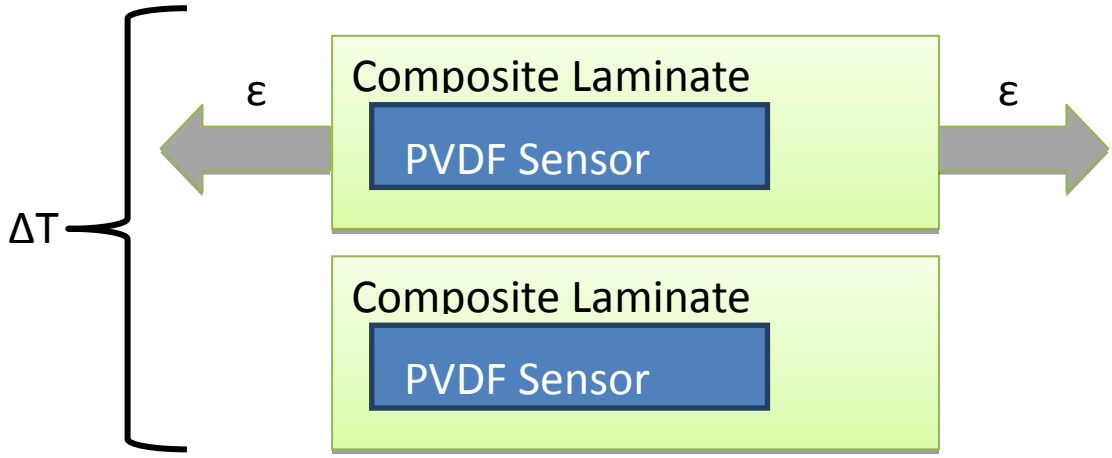

Figure 13: PVDF sensor temperature compensation setup using a half-bridge

In this setup, the two laminates undergo the same temperature change, but only one is strained. Thus, when the results are analyzed, the results from the unstrained sample may be subtracted from the strained sample, and the difference will give the true strain, with no temperature effects present.

DATA ACQUISITION

Hardware

All sensors were wired into their respective bridge and charge amplifier circuits on an engineering breadboard. The outputs from these circuits were connected to a National Instruments USB-6229 data acquisition board (DAQ). The board enabled voltage readings to be gathered from the bridge and charge amplifier circuits, which could then be converted into strain readings. The DAQ also enabled direct wiring of the thermocouples in order to gather temperature data. The DAQ specifications are shown below in table 5. An important consideration when choosing testing equipment is whether it is accurate enough to capture small variations in the data being collected. Due to the small voltage changes seen in the Wheatstone bridge, the highest resolution DAQ that was available was utilized. The specifications for the different measurement settings used are shown in table 6. These specifications affect the error of measurement. These will be further discussed in the error analysis section of this document.

Table 5: DAQ specifications for measurement

DAQ Model	Bits	Sensitivity +/- 50mV	Sensitivity +/- 10V
NI 6229USB	16	5.2 µV	97.6 µV

Table 6: Resolution and sensitivity for inputs

Source	Resolution	Min. Sensitivity	Max Error
MFSG Bridge	0.1 µV	5.2 µV	+/- 5.3 µV
PVDF Bridge	30.5 µV	97.6 µV	+/- 128 µV

Software

All of the data gathered by the DAQ was collected and transcribed utilizing a custom National Instruments LabView program. It is important to note that all data presented in the results section of this work was taken directly from raw data collected by LabView from the sensor outputs, and converted to strain measurements in a separate program. However, the LabView program was written to include an additional interface that converted the data to strain, and displayed it on a real-time graph. This was to ensure that, during testing, problems with the testing, circuits, or programming could readily be identified and rectified. Block diagrams of the raw acquisition program can be seen in figures 14 and 15.

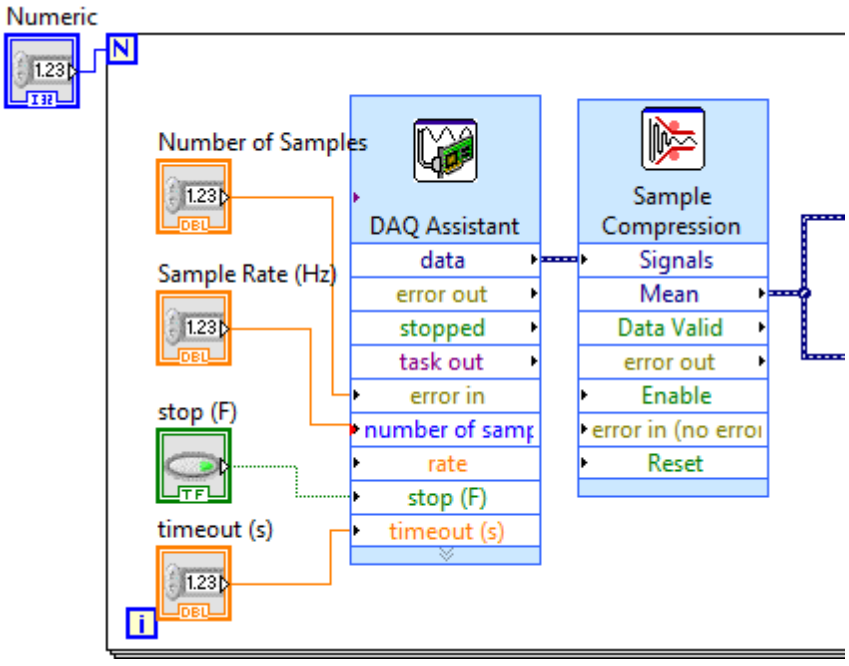

Figure 14: Data collection interface (1/2)

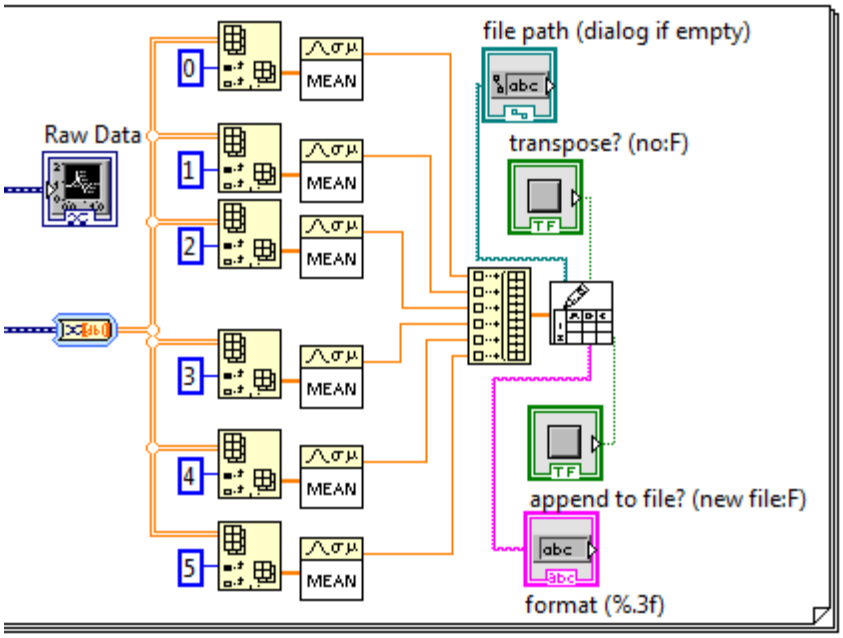

Figure 15: Data collection interface (2/2)

The outputs from the Wheatstone bridge and charge amplifier circuits are voltages. Thus each channel measuring these values was set to measure voltage differential (with respect to the circuit ground). The power supply voltage was also monitored, to ensure that results obtained were not a result of fluctuations in supply voltage. The thermocouple output is also a voltage differential. LabView has preprogrammed settings tailored to specific thermocouple types. The DAQ Assistant channel strips were set up with the parameters shown in Table 7.

As can be seen from Figure 14, once the raw data was made available to the channel, the DAQ Assistant channel strip allowed the selection of the channel sample rate, total number of samples to take, and a timeout and manual stop feature. From here, some signal compression was applied, and the mean of all samples taken within each

sample period was taken. This removed some of the noise from the data. From this step, the data was sent to two locations.

Table 7: DAQ Assistant Channel Settings

Signal Source	Output	Range		Measurement Type
		Max.	Min.	
Thermocouple	Millivolts	-	-	25 CTC (LabView Default)
MFSG Wheatstone Bridge	Millivolts	-50	50	Differential Voltage (with respect to circuit)
PVDF Charge Amplifier	Volts	-10	10	Differential Voltage (with respect to circuit)
Power Supply	Volts	-10	10	Differential Voltage (with respect to circuit)

One copy of the raw data was appended directly to a spreadsheet file, and the other copy was processed within LabView to provide a real-time graphical reference of the data, to ensure that reasonable data was being accumulated, and for general monitoring purposes. All of the data presented here was processed manually from the raw spreadsheet data. The analysis of this data can be found in the data analysis section.

MANUFACTURING PROCESSES

Vacuum Assisted Resin Transfer Molding Process

The method of laminate construction utilized for this process was vacuum assisted resin transfer molding (VARTM). This method was utilized because it closely resembles the actual method used in constructing wind turbine blades. In VARTM processes, the composite is laid up in the desired configuration inside of a sealable mold. In this case, the mold was made up of a flat aluminum plate upon which the composite sheets were placed. The mold can be seen in figure 16.

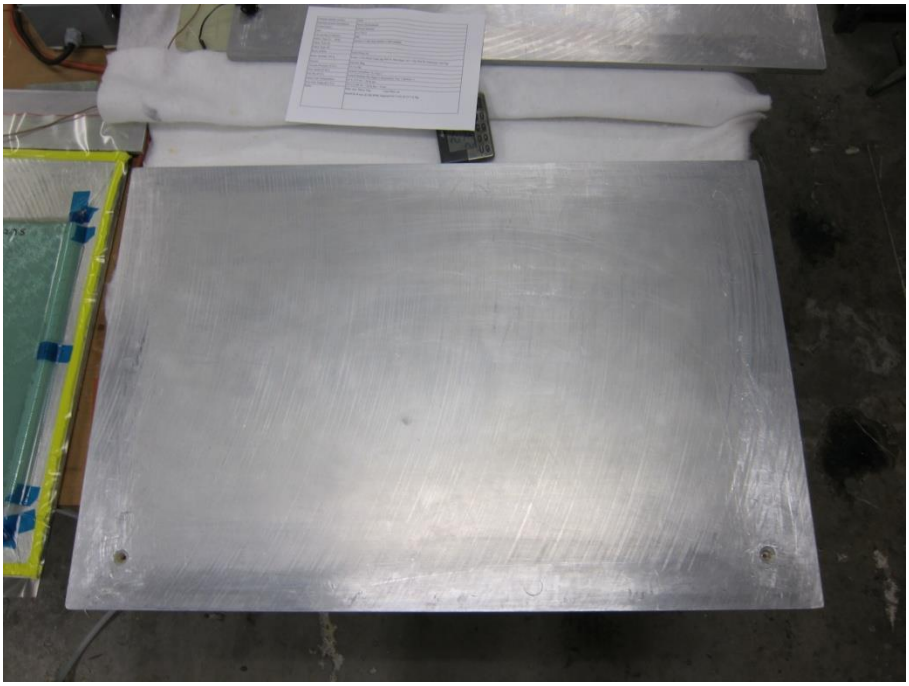

Figure 16: Flat aluminum plate VARTM bottom mold

The other half of the mold is made up of a “bag” which is thin plastic sheeting that is placed over the top as seen in figure 17.

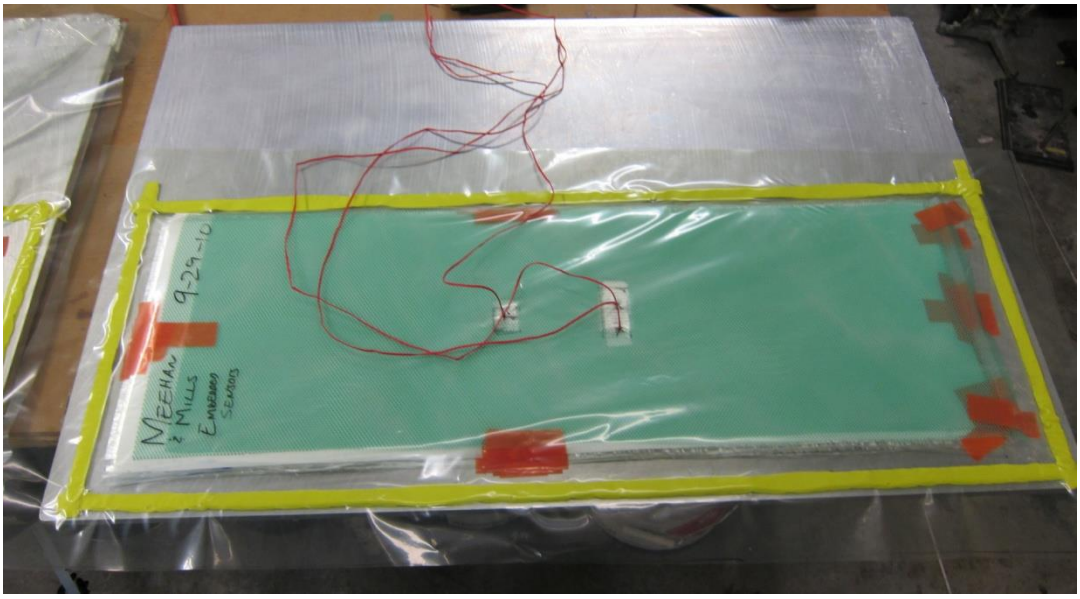

Figure 17: VARTM Layup with bag overlay

It is sealed with the use of Tacky Tape®, a butyl sealant tape applied around the edges of the mold. This can be seen in figure 18.

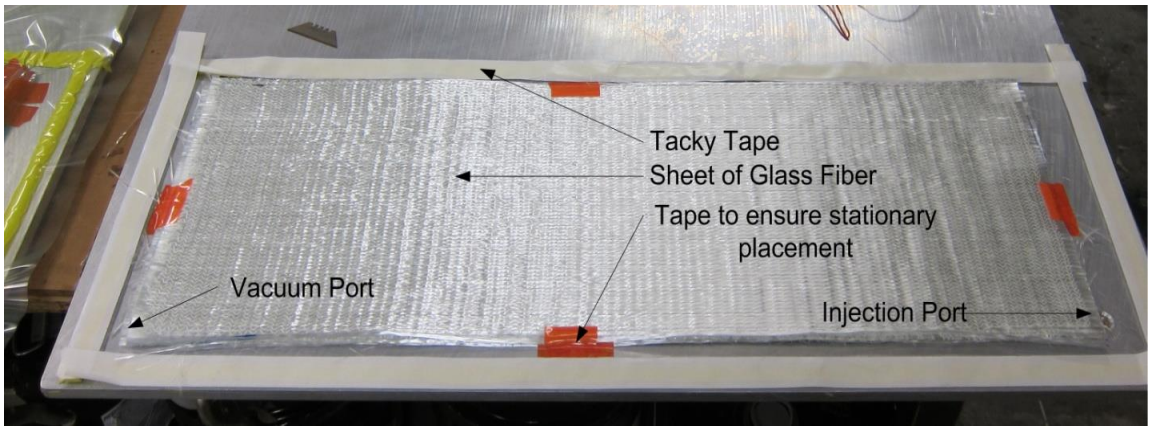

Figure 18: VARTM layup and mold with plies laid up

The composite layup involves several different parts in this process. First, a release agent is applied to the aluminum plate in order to facilitate removal of the plate after the resin cures. Then a peel ply is laid down, which can be seen in figure 19.

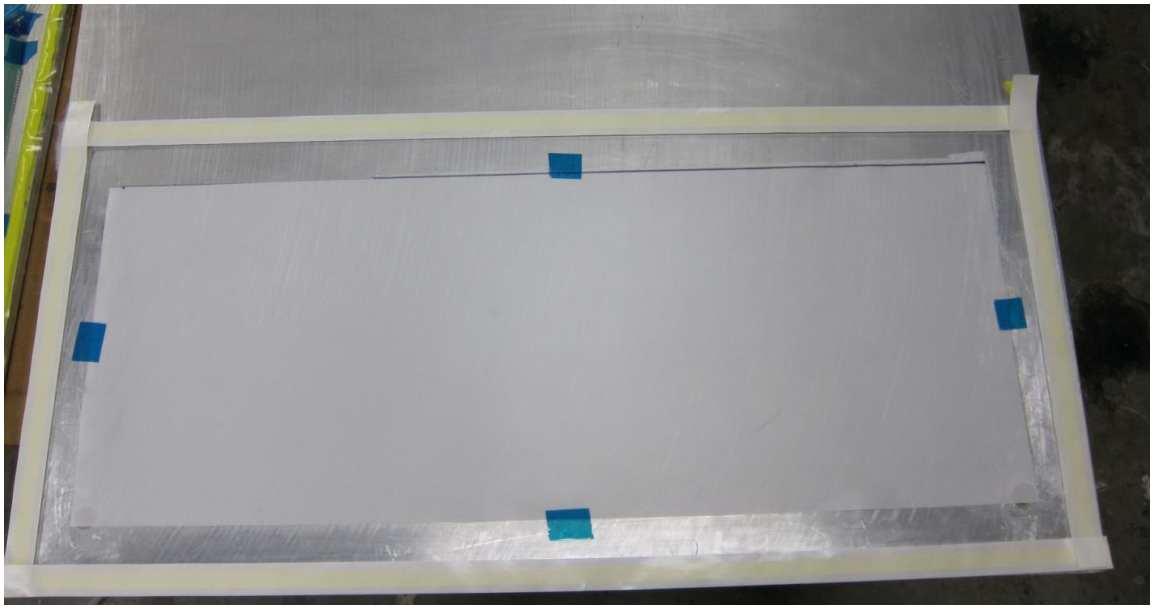

Figure 19: Mold plate with peel ply layer

Peel ply is a polyester fabric that facilitates easier release of the composite laminate from the mold. The peel ply is easily stripped from the laminate after cure. The matrix plies of the composite are then layered in the desired configuration. In this case, relatively thick (9-ply) laminates were constructed with all plies oriented in the principal direction. After the plies were layered, and additional layer of peel ply was laid down to facilitate release from the flow media, which is pictured in figure 20.

Flow media is an extruded plastic netting that is laid down on top of the laminate stack. The purpose of the flow media is to facilitate faster resin impregnation of the laminate.

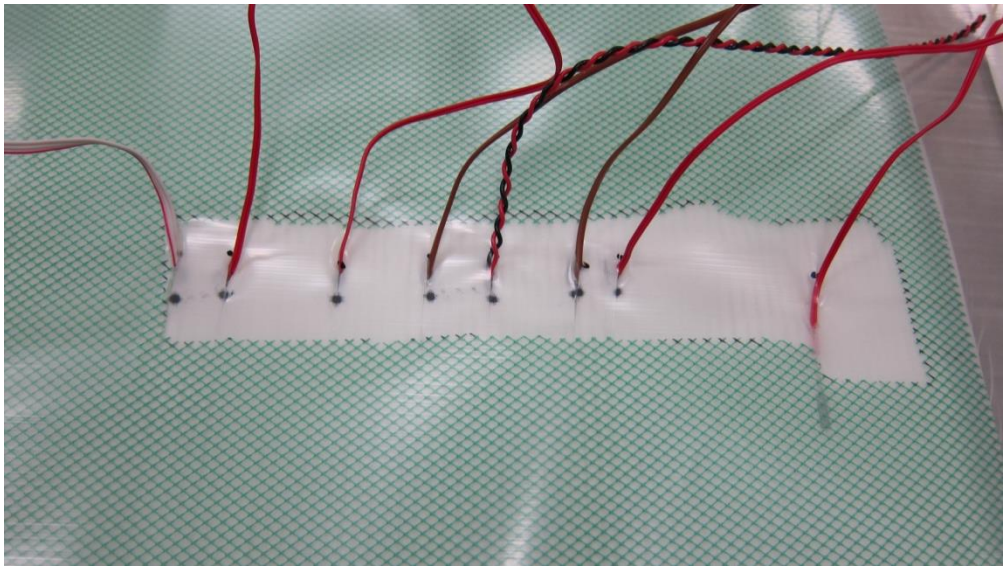

Figure 20: Close-up of sensor wires showing flow media

This works by allowing the resin to flow readily along the top of the laminate, and flow downward through the plies, rather than flowing through the plies themselves throughout the entire process, which would be quite time-consuming.

After the flow media is applied, a plastic sheet (bag) is applied over the top of the laminate stack and sealed to the mold plate via the Tacky Tape. A completed three-ply mold is shown in figure 21 for reference.

Once the mold is completed, vacuum is applied to one end of the mold via a port, shown in figure 18. Once all air is removed from the mold, the vacuum is maintained, and the injection port is opened to a resin source. The vacuum pulls the resin slowly through the laminates. Integrity of the vacuum bag and edge seals is crucial, as any air leaks lead to porosity in the composite, which adversely affects the structural integrity of the composite.

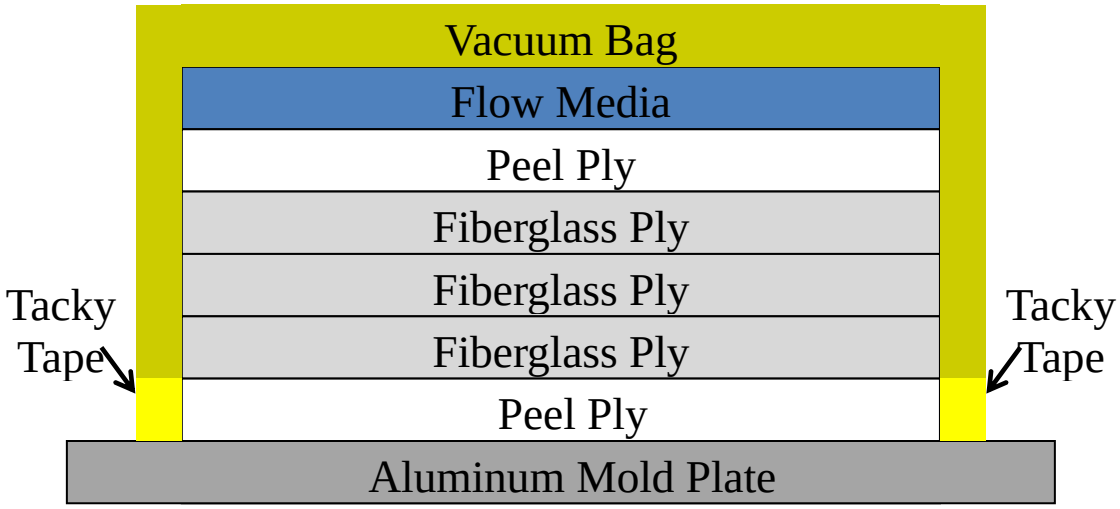

Figure 21: A completed three-ply composite layup in a VARTM mold

When resin has successfully impregnated the entire layup, both ports on the plate are sealed, and the mold is left under vacuum for the duration of the resin cure period.

Sensor Embedment

The sensors used in this work were placed within the laminate during the layup process. Several test plates were manufactured in order to determine the best method of placement. Additionally, the work of Palmer was referenced when placing sensors.

Sensor Treatment

The sensors were surface treated before placement in accordance with suggestions given in Palmer's thesis. The purpose of this treatment was to improve bonding of the sensors, and reduce structural weaknesses as a result of the sensors being embedded.

The treatment process involved several steps. First, the sensors were cleaned using isopropyl alcohol. Then they were dipped in a 20% by weight solution of nitric acid for ten seconds. Finally, they were rinsed with water.

Sensor Placement

The sensors were placed in the fifth ply of the 9-ply laminate. The laminate was constructed simply with all plies in the principal direction, or $[0]_9$. Five layers of the laminate were layered, and then the sensors were placed in that layer, as shown in figure 22.

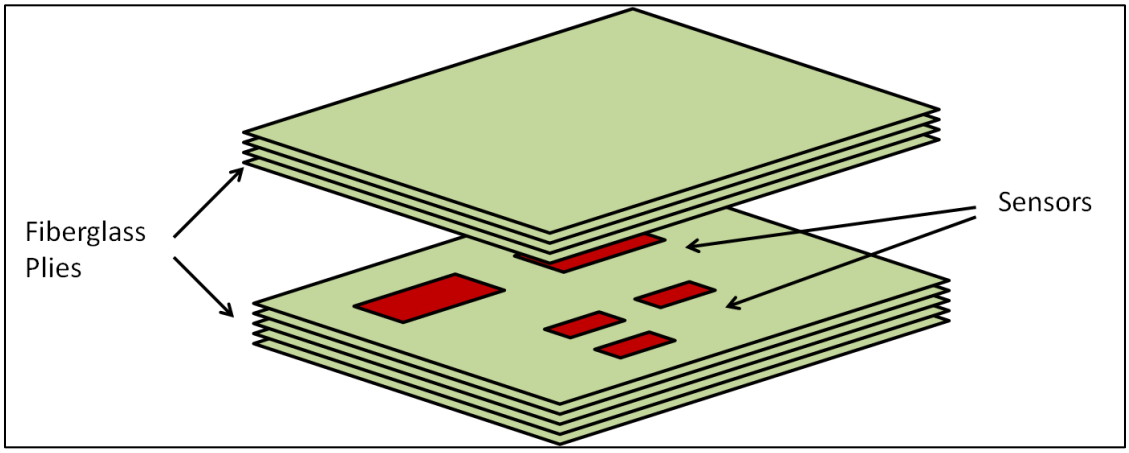

Figure 22: Visual depiction of laminate layup including sensors position.

Sensor placement and alignment is an important factor in measuring composite strains, due to the anisotropic nature of most composite materials. In these tests, unidirectional fiberglass mat was used, so the major mechanical properties were along the principal direction of the laminate. Thus, most sensors were aligned in the principal direction, and the majority of data recorded was in this direction, as is seen in figure 23.

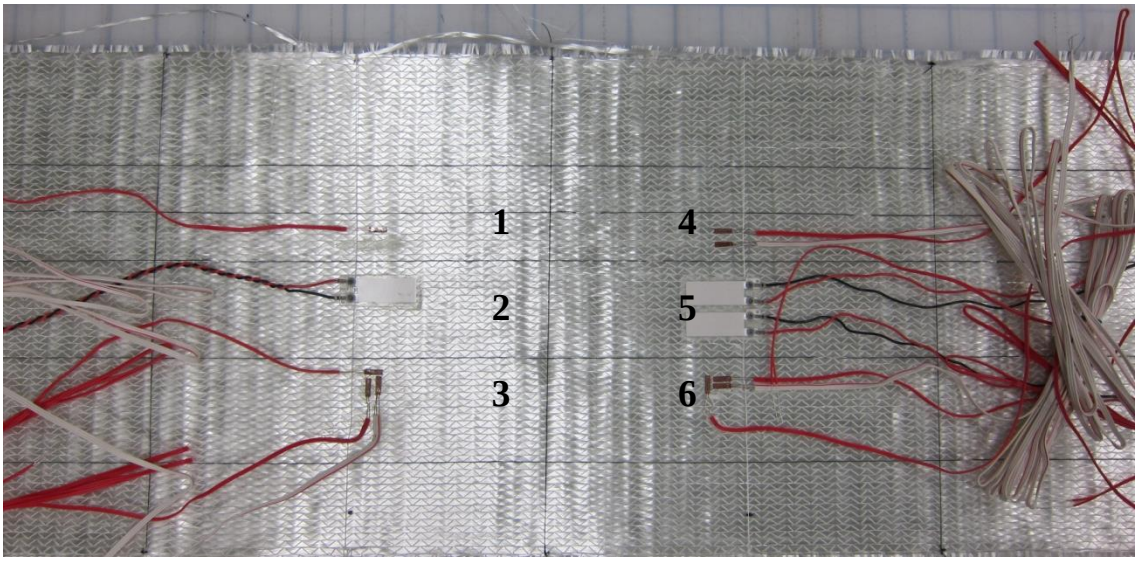

Figure 23: Middle ply with embedded sensors (final “master” plate)

From the above figure, it can be seen that multiple sensor configurations were utilized within the laminate. The following table 8 lists the sensor configurations that correspond with the numbers on the photo:

Table 8: Sensors and configuration

Reference Number	Sensor Type	Configuration
1	2- Wire MFSG	Embedded Quarter Bridge
2	PVDF	Embedded Quarter Bridge
3	3-Wire MFSG	T-Style Half Bridge, 2 Direction
4	3-Wire MFSG	Embedded Quarter Bridge
5	PVDF	Embedded Half Bridge
6	3-Wire MFSG	T-Style Half Bridge, 1 Direction
Additional Sensors		
	3- Wire MFSG	Surface Mounted Quarter Bridge
	2- Wire MFSG	Surface Mounted Quarter Bridge

Sensor Wire Extraction

Once the sensors were placed, the wires were then woven up through the additional plies, as can be seen in the figure 24. This was done by spreading the tows slightly and pushing the wire through the ply.

Once the final four plies were layered in this way, the top peel ply, flow media, and bag were layered. Since the cure process was to be monitored, it was necessary for the sensor leads to be accessible outside of the mold. This posed a unique problem. The integrity of the mold was compromised by extracting wires from it. In order to best maintain the integrity of the mold, and to reduce leakage, a method of double-bagging was developed. Nearly all cure monitoring sensor research that has been done by others concentrates on fiber-optic sensing, including several reports focusing specifically on sensor egress points (18), (27).

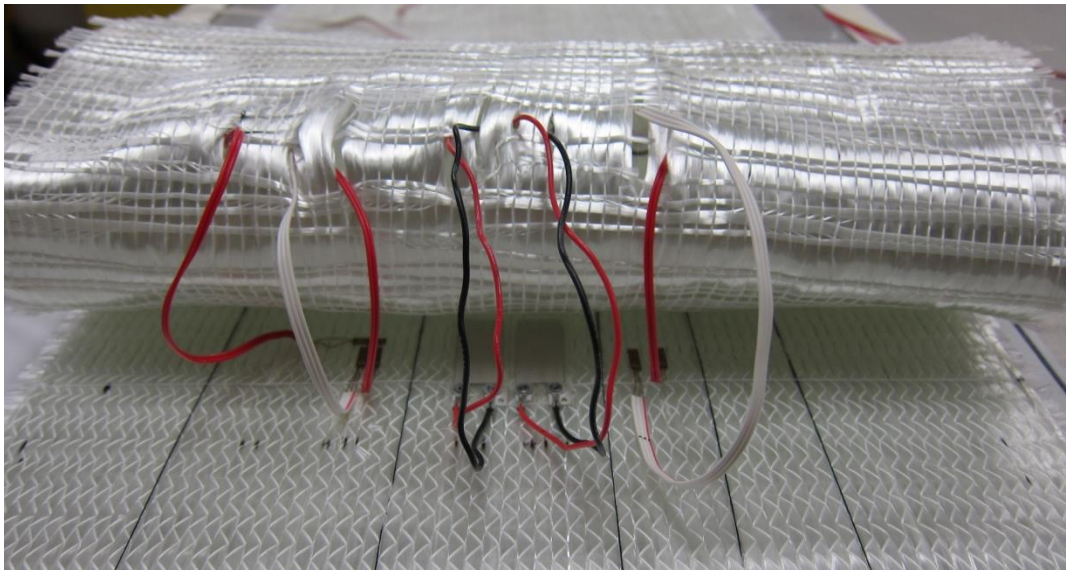

Figure 24: Ply with wires woven through

However, methods for standard sensor wire extraction have not been developed. In the work of Crasto et. al, the wires were simply placed along the top of the plate, and fed through the mold tape (21). The same process was initially used by all of the researchers at MSU. While Crasto makes no mention of failures due to this method, the researchers at MSU have found this method to be unreliable for several reasons. Air ingress at the sensor wire-mold tape interface was found to be a major issue. Furthermore, many of the sensor lead were too short to access the side of the mold. On a large layup, such as a wind turbine blade, this would become even more of an issue. Finally, as the wire was laid across the top of the mold, it created a barrier for resin flow, and caused a resin buildup. This led to undesirable resin flow process, and an undesirable plate finish. As no developed documented method for wire egress systems is apparent, a portion of this research project was devoted to proper sensor wire egress methods out of the necessity to access the sensor wires during the resin infusion process. This process is outlined as follows:

First, the flow media was cut out in the area surrounding the wires. This slowed the resin flow and ensured minimal porosity would occur. Then, small slits were cut in the top mold bag, at the wire locations, and the wires were inserted through them as shown in figures 25 and 28.

Next, a layer of Tacky tape was applied in a small rectangle around the compromised area of the top bag. The sensors wires were firmly pressed into this layer of tape, and a second layer of Tacky tape was applied, essentially sandwiching the wires.

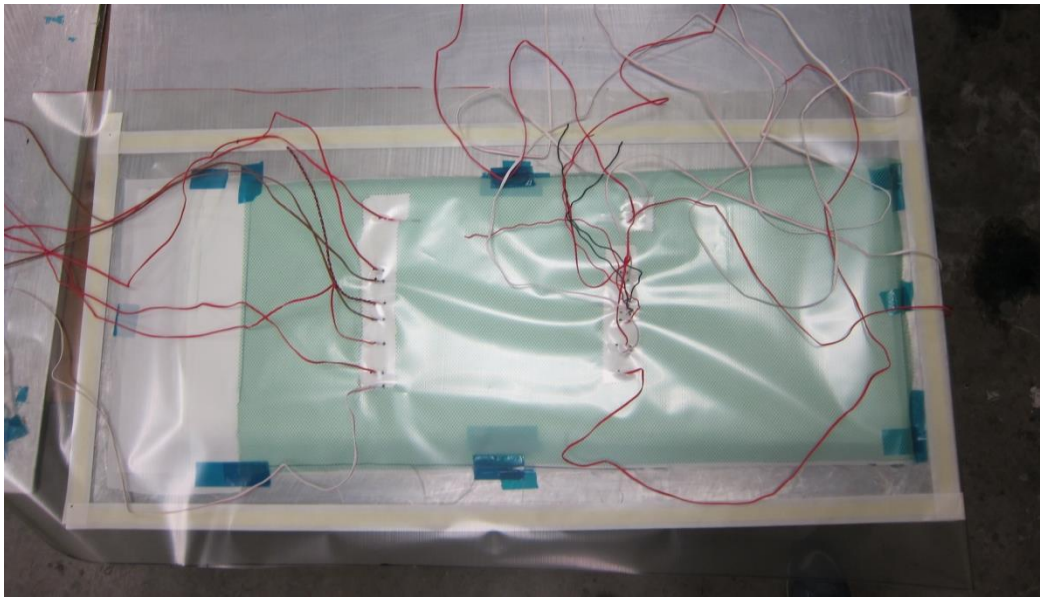

Figure 25: Lead wires inserted through outer bag

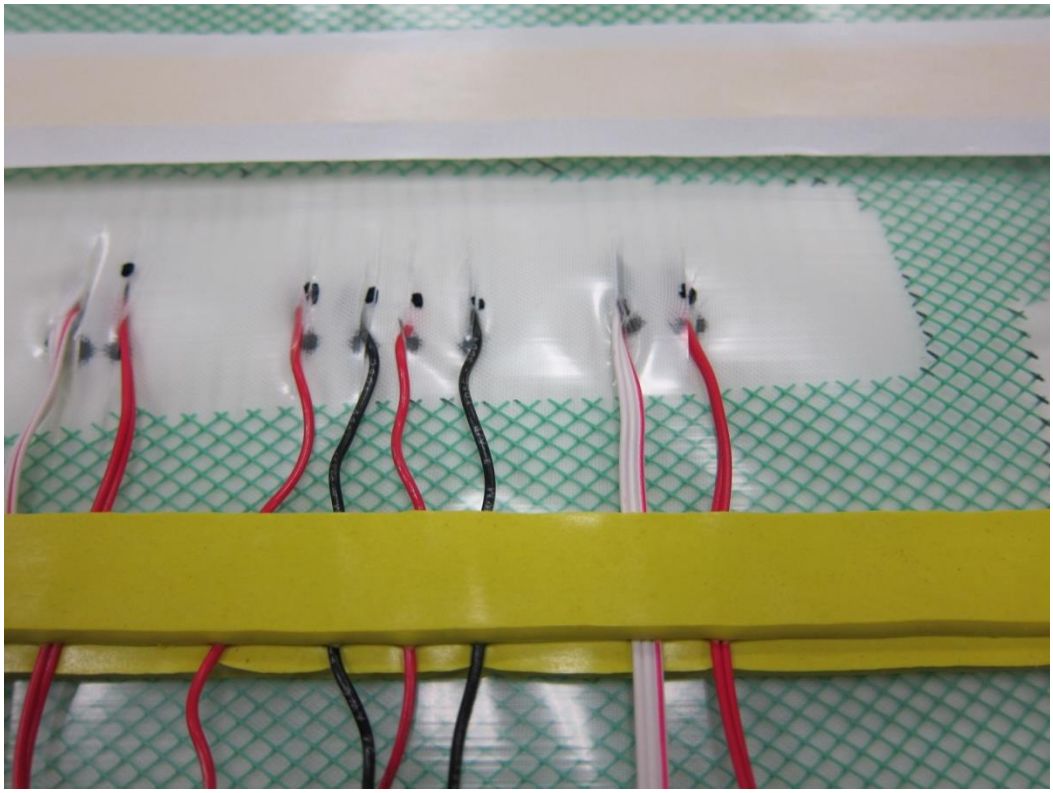

Figure 26: Lead wires sandwiched between Tacky tape layers

The tape was firmly worked and compressed around the wires to guarantee an airtight seal, which is shown in figure 26.

Finally, a small piece of bag material was cut and placed over the second layer of Tacky tape and sealed, as seen in figure 27. This allowed for access to the lead wires, and still yielded good mold integrity. Additionally, if any problems were indicated during the vacuum test phase, the problem area was minimized to one or two locations. Incidentally, the wires themselves were a source of air ingress, and that was also addressed (see Mold Testing below).

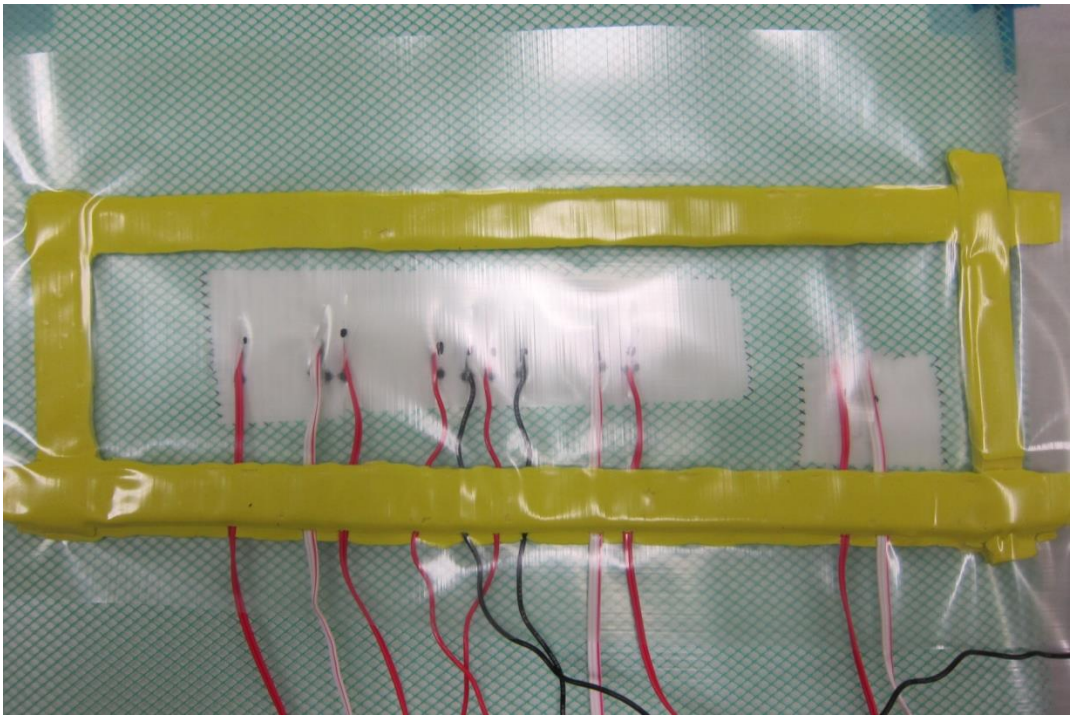

Figure 27: Second bag overlay

This process of double bagging for sensor wire egress yielded 100% mold integrity over the course of this research and the eight molds that were manufactured.

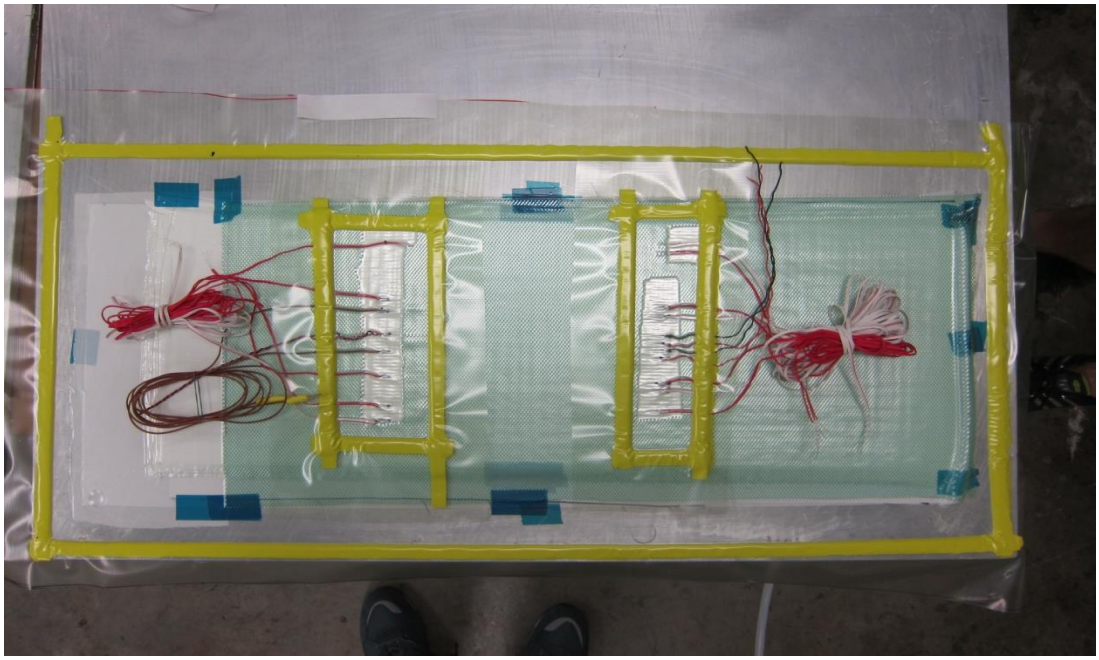

Figure 28: Completed testing layup

Mold Testing

It can be seen that the layup process is very time consuming. It is also expensive, as once a plate is shot, none of the sensors or materials may be reused. Thus it was crucial that part of the process was testing the integrity of the mold, to ensure that no air ingress occurred. In order to test the mold, vacuum was applied to the mold until steady state vacuum of approximately 29 in-Hg was reached. The ports were then sealed, and the mold was left for a period of twenty-four hours. The mold was then examined to see if air leakage had occurred.

Several issues were identified in this process. The first issue was leakage around the lead wires at the Tacky-tape seam. This area was resealed, re-tested and found to be satisfactory. The second issue was air ingress via the wire insulation conduits. A surprisingly large amount of air was being drawn in through the wire leads. The open end

of every lead was consequently sealed, and the integrity of the mold was found to be satisfactory.

Composite Material

The composite plates constructed for this testing were 9-ply fiberglass plates with all laminates laid up in the one direction. The fiber material used was Saertex U14EU920-00940-T1300-100000 Unidirectional. The matrix material used was Gurit Prime 20LV Resin. A normal rate hardening agent was used, yielding a working time of approximately 20 minutes. The curing process of the resin was highly exothermic, causing some working issues including melting of plastic pipes and fittings used to inject the resin. This configuration was chosen due to ready availability, ease of testing, and similarity to manufactured wind turbine blades.

Injection Process

The process of resin injection was complex due to the relatively thick nature of the plates being constructed. Trial and error was used to determine the best rate of injection. On the first manufactured plates, a combination of large PVDF sensors and too high of an injection rate caused severe porosity problems near each PVDF sensor, even though the mold integrity was satisfactory. This can be seen in figure 29. The reason for this localized porosity can be best explained by figure 30. The resin travels more slowly when contacting a solid object such as a sensor, based on its fluid properties. This caused resin flow to slow down near the sensor, and left a void near the end.

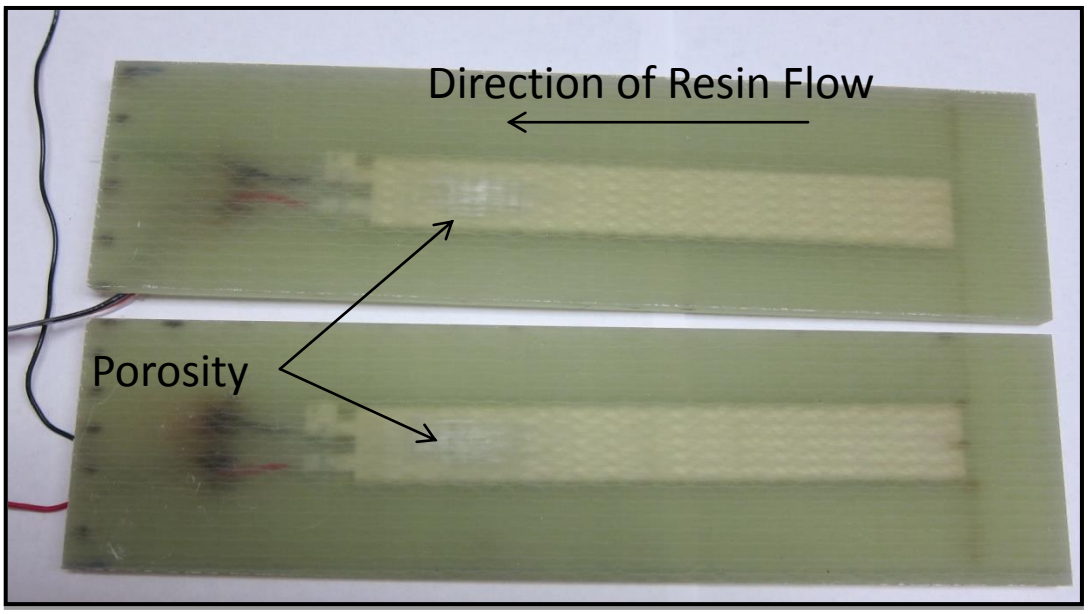

Figure 29: Porosity Under PVDF Sensors

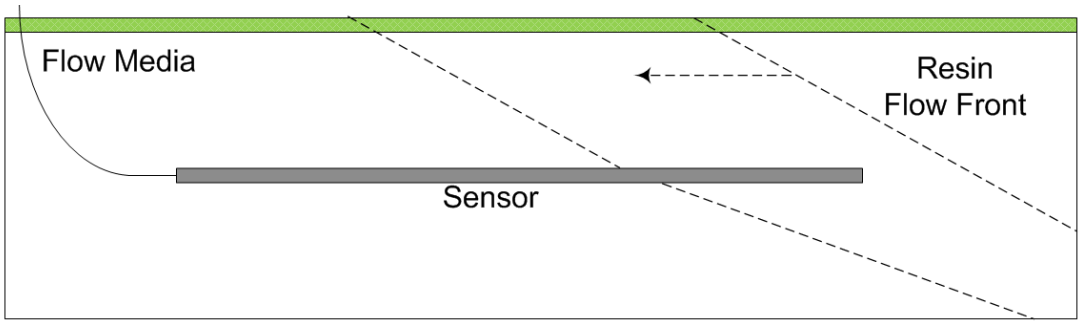

Figure 30: Illustration of resin flow front slowing near sensor.

Cure Process

Once a satisfactory rate of resin injection was determined, a full test plate could be produced. The cure process was one of the key areas for which stress/strain data was desired. Once the plate is fully injected with resin, it is left to cure at room temperature for 24 hours. It is then placed, still attached to the aluminum mold plate, into an industrial oven, and cured for 12 hours at an elevated temperature. Once this was completed, the

plates were removed from the mold, peel ply and flow media were removed, and the plates were cut into coupons for further testing for Ed Meehan's research.

Thermoset resins, such as the one used here, typically set in two steps. The resin is injected in liquid form. As the polymers that make up the resin begin to cross-link, it enters a gelation stage. This is essentially when the resin is no longer liquid, but becomes a flexible, three-dimensional solid. It still has low mechanical strength properties, but can no longer be manipulated without compromising the final composite (28). From the gel stage, the resin continues to cure until it reaches its final mechanical properties, which are significantly stiffer and higher-strength than the gel stage.

TESTING

Room-Temperature Cure

Data acquisition was begun with the start of resin injection. The data from the actual injection process was not useful, but was used to establish a baseline. Data was collected for the first twenty-four hours of room-temperature cure. It can be seen from the data that the first twenty hours was the most significant as far as creating residual stresses and strains within the composite. After this point, further data revealed no change to the plate.

Even in room-temperature cure situations, it was necessary to use temperature-compensated strain gages. As was previously mentioned, the resin exhibited a strong exothermic reaction, and caused the plate to heat up considerably on its own during room-temperature cure.

Elevated-Temperature Cure

The elevated temperature cure testing presented a couple of unique challenges. After making a few test plates, it was apparent that purchasing strain gages with extra long leads would be advantageous, as the plate must be placed in an industrial oven, and the leads to the DAQ had to egress out through the door joint. Here also, it was very important to utilize temperature-compensated strain gages, in order to separate the added thermal effects of the oven.

Testing Plan

In order to organize the workflow, a testing master plan was created. Each major step was seen as a milestone for the work to continue. Each step was completed to satisfaction before the next step was begun, in order to work more efficiently. The main testing points can be seen in the table 9.

Table 9: Testing Plan

Laminate Cure Testing		
Step	**Test**	**Special Action Required**
1	Sensor Output	Static Tests to Determine Outputs
2	Sensor Output	Static Tests to Remove Noise
3	Laminate Layup	Test to Determine LabView Parameters
4	Full Laminate Test	Full Test for Data Purposes
5	Master Plate	Master Plate for Final Results

Each of these steps involved careful planning, and assorted tests within themselves. These are explained in detail as follows:

Step 1: Determining Outputs

Each sensor type was fully researched, and the appropriate sensors were procured. The technical specifications for each were carefully studied and understood before any testing was begun. Once the sensors were obtained and understood, the initial data acquisition programs and related circuits were constructed. Simple, uncontrolled tests were performed at this point, only to determine what kind of output, if any, could be expected from the sensors. Little was done to quantify MFSG outputs, as they are proven technology, simple, and well understood. More attention was given at this point to the

PVDF sensors, as there exists much less documentation of their usage for long-term strain testing ability. After much work on the LabView program and the circuits and simple testing, it was determined that the sensors were well enough understood for the first round of real testing.

Steps 2 and 3: Removing Circuit Noise and Laminate Layup

An attempt was made to forge quickly ahead with the research once reasonable results from the initial testing were being established, and the first laminate was made, as a test for the circuits, and to be used to characterize sensor output. Upon review of the data, it was determined that, while trends in the data were apparent, far too much noise was being exhibited by the sensors. The laminate was sliced into testing coupons, each containing several of the sensors, and these were used both for characterization of the sensor outputs under various loadings, and as good embedments for the sensor for further circuit refinement.

The LabView program was re-programmed to better represent long-term trends, and reduce noise in the represented data. The program was designed to plot data points that were aggregate of many other points measured. This better represented the true values, and clearly showed trends in the data.

The circuits were redesigned, utilizing higher quality components, better solder joints, and more reliable power supplies. The initial power supply that was utilized would fluctuate over time, and caused many undesirable results. A backup power supply was added to the testing equipment, to account for surges in the laboratory power supply, as elevated temperature cure data was lost for the first two plates due to power outages.

Also, in this phase of the project, the heating tests on both sensor types were performed. Due to the nature of the industrial convection oven used, minute temperature fluctuations were apparent in the data. Different methods of testing and specimen placement were utilized to overcome this.

Tensile tests were also performed on the specimens, to determine sensor response and output, in a laminate loading scenario. In this phase of testing, much about the characteristics of the sensors was determined. The full sensor testing matrix can be seen in Appendix A.

Step 4: Full Laminate Test

Once clean and reliable data was being established by the LabView programming, related circuits, and sensors, a full laminate was produced with several of each type of sensor (PVDF and MFSG) embedded. This was to be the basis for the final test. Data was recorded for the entire room temperature cure process, as well as the elevated temperature cure test. Unfortunately, testing with the 3-wire strain gages was not completed by this step, and all data was representative of 2-wire gages with resistive heating drift. Even though temperature affected the results somewhat, a clear trend was seen towards permanent compressive strain, as a result of the thermochemical shrinkage in the room temperature cure process. For this testing, the elevated temperature test showed no change in the residual strain. This was later evidenced by the master plate.

Step 5: Master Plate

Now that clean, reliable data was being accumulated, and the expected results from the cure process were being realized in the data, a final master plate was made. This

plate was large, and included all of the sensors necessary for both the cure monitoring, and also for testing later for Meehan's work in health monitoring. It was at this time that the testing for the three-wire MFSG gages was completed, with excellent results, and these were utilized in this testing. Also, smaller PVDF sensors were used, to avoid the porosity issues previously discussed. The data collected from this master plate is very reliable, and all MFSG circuits trended similar results. These are presented in the following results section.

RESULTS AND ANALYSIS

PVDF Sensors

The first portion of the testing plan involved testing sensor outputs in order to establish baseline values and determine expected output values. The PVDF sensors and their respective charge amplifier circuits were constructed and tested. Several issues were readily identified that severely limited the use of these sensors for the determination of residual stress/strain testing.

Since PVDF sensors indicate changes to their shape by emitting a charge, they are susceptible to charge decay. This turned out to be a significant issue, since most of the testing done was at essentially steady-state timeframes. Testing was performed with altered loading rates and time constant circuits, but ultimately it was decided that for cure monitoring, PVDF sensors could not be used.

PVDF Loading 1: Bending Test

The first test performed on the PVDF sensors was a simple bending test. The reason a bending test was chosen was that early on, simple characterization of the sensors was desired. A bending test would produce large stresses, which would clearly chart the response of the sensor.

In this test, the sensor was fixed to an aluminum bar that was clamped on one end, and a 20N force was applied instantaneously, in a cantilever beam loading scenario, as shown in figure 31.

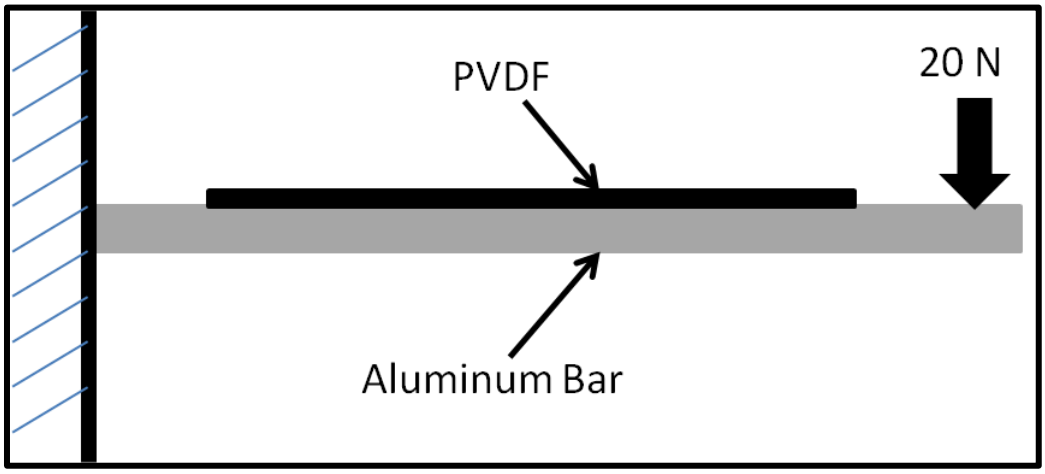

Figure 31: Depiction of PVDF cantilever bending test setup

Figure 32 shows the results of the bending test.

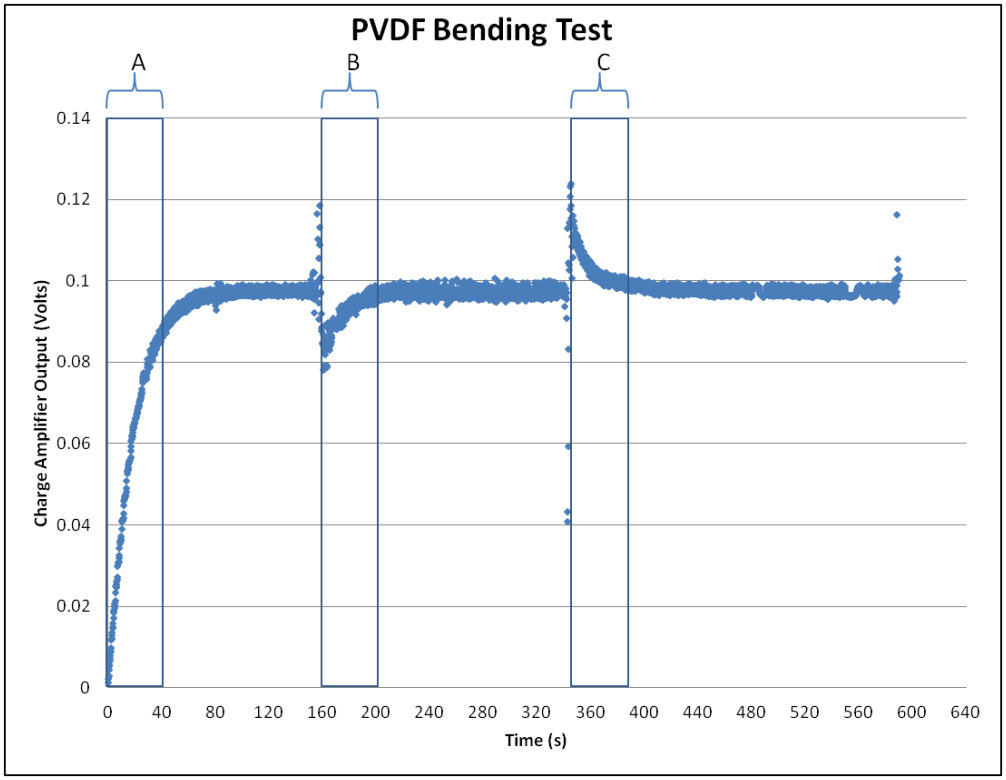

Figure 32: Output from PVDF during bending test showing decay of charge as load is held.

Each boxed region on the chart represents the 40 second time constant of the charge amplifier circuit that was used in this test. Region (A) represents the initial charging of the capacitance of the circuit. Once the circuit was at steady state, the 3.5 N-m moment was applied (Region [B]), and the strain change can be seen in the approximate 20 mV drop in the charge amplifier circuit voltage. The loading was held constant until Region (C). Notice that even though the load remained constant, the charge decayed until the circuit was once again at its steady state operating condition.

The loading was then removed instantaneously at Region (C). Here, an equal and opposite 20mV change is seen in the circuit, and then that also decays to the steady state condition. So the circuit essentially resets itself back to null within the time constant of the charge amplifier circuit. Thus, long-term steady-state monitoring is not supported by PVDF sensors. Attempts to increase the time constant only reduced the sensitivity of the sensors.

PVDF Loading 2: Tensile Testing of PVDF Sensors

Since the sensors were to be utilized in cure monitoring to measure axial strain in the principal direction of the composites, it was desirable to also test the PVDF sensors in an axial strain situation. The test involved adhering a PVDF sensor and an MFSG sensor (for reference) to an aluminum bar. The bar was used as a test fixture as the sensors are too fragile to be tested directly.

The aluminum bar was then clamped into an Instron 5882 tensile tester and loaded at a constant rate, paused and held, and then unloaded. The resulting sensor ouputs can be seen in figure 33. The loading profile of the test coupon is shown in figure 34.

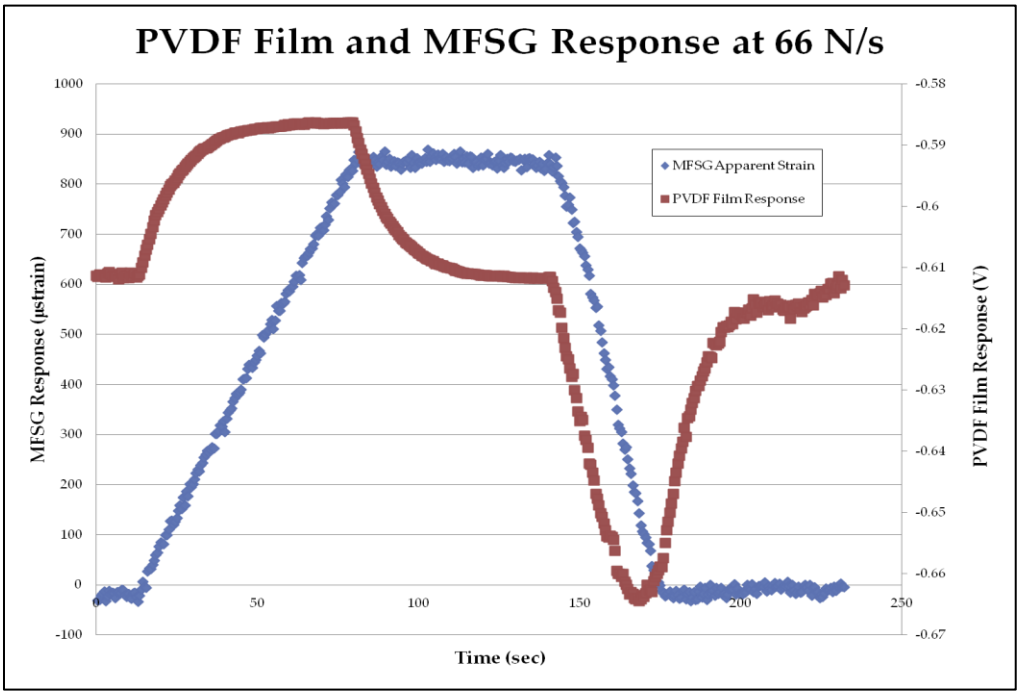

Figure 33: Response of PVDF and MFSG in axial tension test.

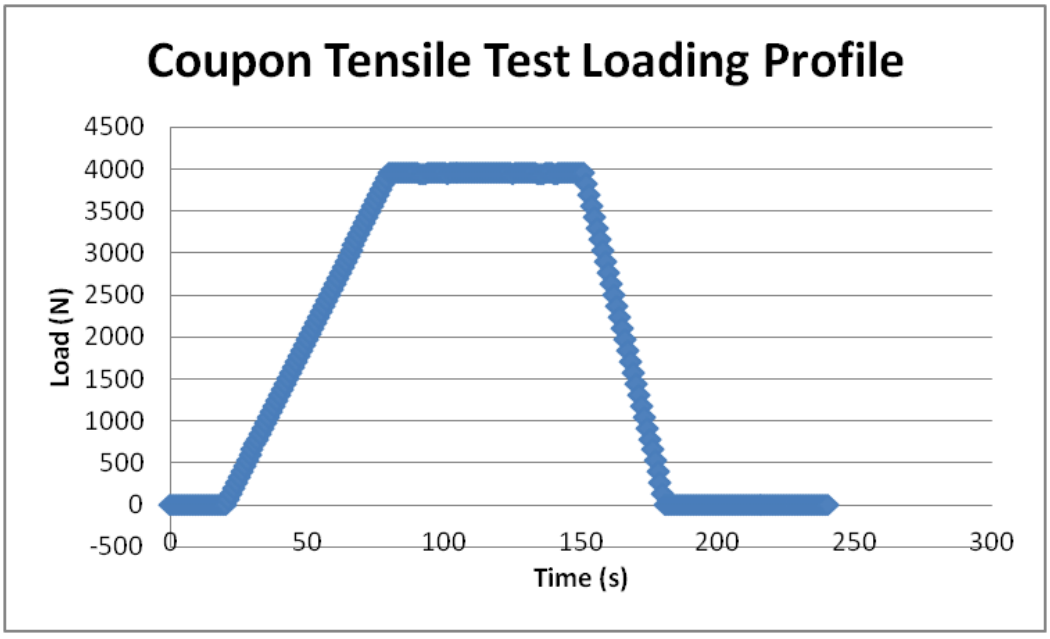

Figure 34: Tensile test coupon loading profile

From figure 33, it is evident that even though the loading rate was constant, the PVDF sensor failed to indicate a constant rate, instead creating a shark fin curve indicative of its capacitive charging characteristic. Once the loading was paused (at about 90s), the charge in the sensor immediately began to decay, back to its steady-state value.

Notice that the sample was unloaded at a faster rate than it was loaded. While the MFSG clearly indicates the true strain, the PVDF indicates two things: A compressive strain, and a higher strain. Thus it appears that the output of the PVDF sensor is dependent on loading rate. This relationship is further explored in the following. Once the load is removed, the PVDF sensor once again decays back to its steady state condition.

PVDF Loading 3: Effects of Rate on Output

Since the tensile testing indicated that the PVDF response appeared to be rate-dependent, it was desirable to more closely examine this relationship. Once again, the aluminum bar with a PVDF adhered to it was used for the testing. The bar was loaded from an unloaded condition, to a maximum load of 4450 N for each test. The load was then held constant until the charge amplifier value decayed back to the baseline value. The results of the tests can be seen in figure 35. Figure 36 gives a typical loading curve for each sample in this test.

The loading curve shown in figure 36 is typical for all of the loading rate tests done. From figure 34, it is apparent that loading rate affects the output of the PVDF sensors, with faster loadings giving a higher output than slower loadings. It should be noted that when loading rates are very low, the sensor output reaches a nearly steady

state. The maximum voltage increases seen from the charge amplifier for each test are compared in figure 37.

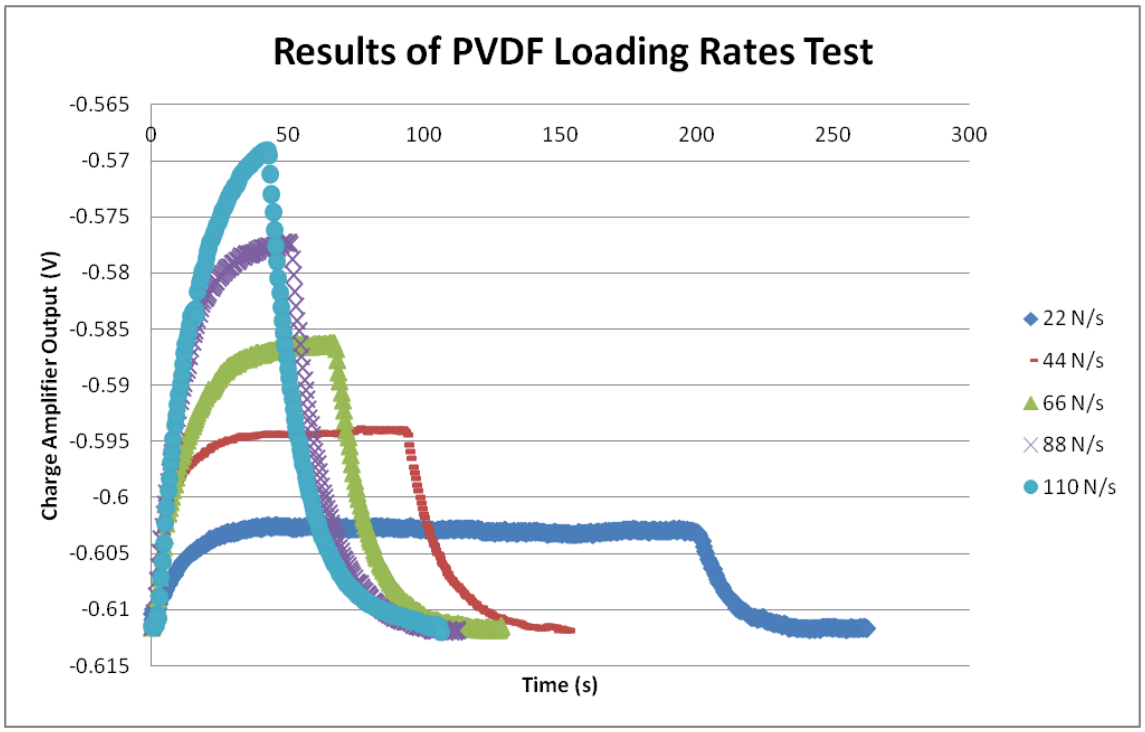

Figure 35: Various loading rates of PVDF sensor, showing different outputs dependent on rate.

When the maximum value increases from the charge amplifier are compared, it becomes apparent that they have a linear relationship, which is a good fit with an R^2 value of 0.9996. Thus it appears that maximum output values can be predicted based on loading rates. Unfortunately, and especially for installation health monitoring applications, loading rates are generally unknown.

Further examination of the data from this test looked into whether the areas underneath the curves, which are representative of the charge density of the PVDF, are equal or simply relatable. These areas were determined and are compared in figure 38.

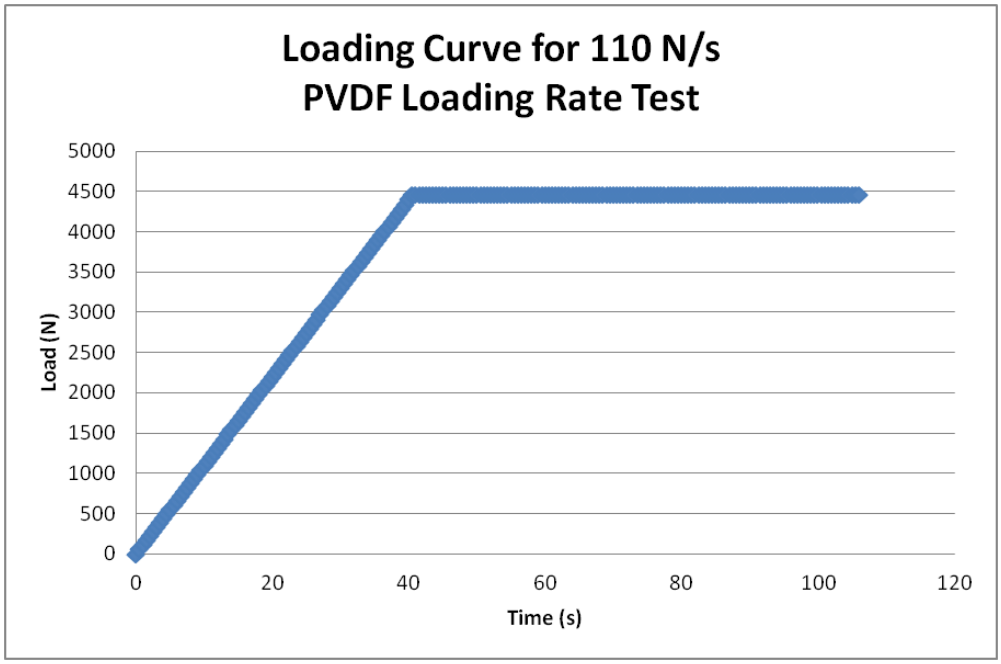

Figure 36: Graphical representation of loading curve for loading rate test

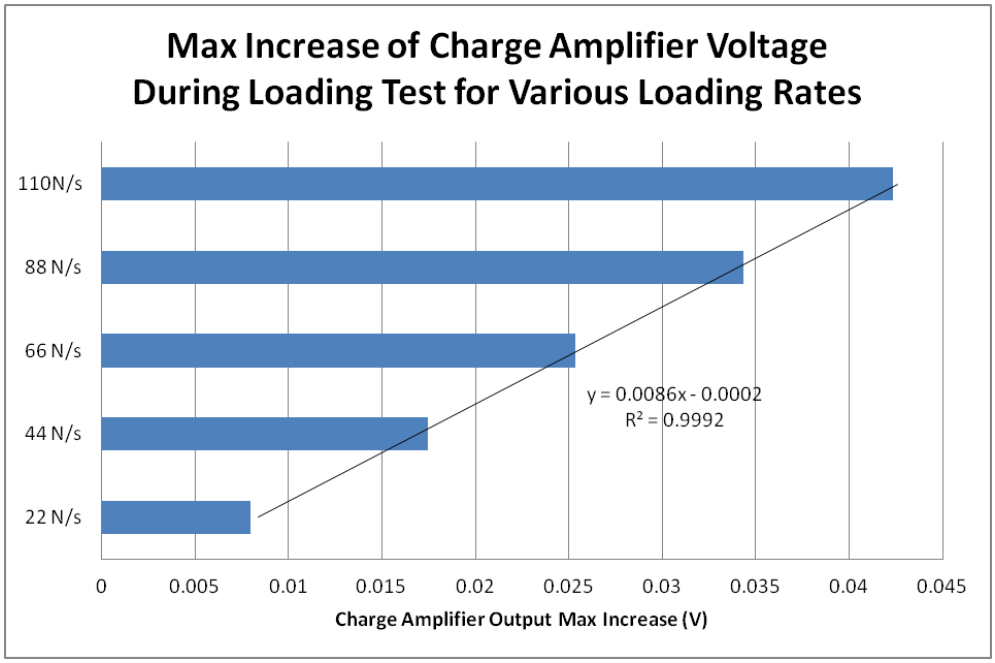

Figure 37: Comparison of maximum increase in values of charge amplifier circuit for the various loading rates.

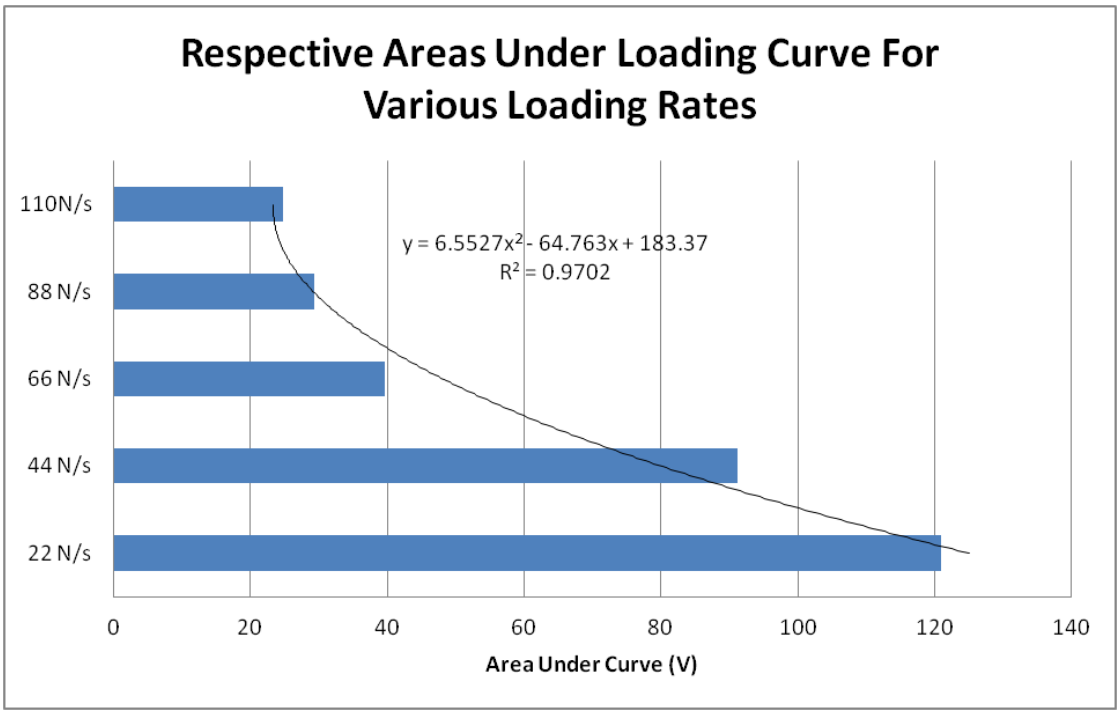

Figure 38: Comparison of areas under curves of PVDF loading rates test.

From figure 38, it can be seen that the area under the curve varies widely for each loading rate, and a useful relationship between them was not established. The best fit regression was a second-order polynomial trend, which is not very accurate. Initial expectations were that these values would be approximately equal. This would be desirable, as loading quantities could be determined by finding the area under each loading curve. Unfortunately, this was not the case, and these tests further proved the limited use that PVDF sensors can provide in health monitoring applications.

PVDFs as Temperature Sensors

The PVDF sensors were very sensitive to temperature changes, which necessitated building some half bridge circuits, in order to retrieve more accurate results. The PVDF sensors can reliably indicate temperature changes. However, just like with

long-term strains, they continually decay back to their initial value over time, after being heated. Thus, in temperature applications also, they cannot be used for long-term monitoring. Meehan, in his work, performed more testing with the bridge circuits and temperature monitoring, and those results may be seen in his thesis.

MFSG Sensors

The rest of this result section will present data from the metal foil strain gages. Since the PVDF sensors proved to be unreliable for long-term testing, all cure monitoring results are based on MFSG results. The results from MFSGs were very accurate and stable. The circuits had very little noise, and the technology is proven.

Post Processing

The raw data from the Wheatstone bridges collected by LabView was appended to an Excel spreadsheet program. From there, post-processing was performed on the data to convert it to strain values. This eliminated error within the LabView program, as only raw values were recorded, and these were separately converted to reflect strain values.

Temperature Separation

One of the first tasks with the MFSG sensors was to reliably separate the temperature effects of the strain gage from the mechanical effects. This was necessary to reduce error and obtain accurate readings. The half bridge and quarter bridge circuits that were described earlier in the circuits section were constructed and tested. The results in figures 39-41 show that temperature effects were accurately removed from the mechanical effects of the strain gages.

In order to test the bridge circuits, a plate was manufactured that had a half bridge, a quarter bridge, and a thermocouple embedded into it. Once the plate was cured, it was cut into a test coupon for use in the Instron tensile tester, and repeated tensile tests were performed on the sample while it was undergoing temperature changes (heating and cooling of the plate section). Figure 39 represents just the quarter bridge strain with temperature. The dips in the data represent axial loading events. From this strain gage alone, it would seem that the strain is steadily increasing and then steadily decreasing, while in reality, just temperature is increasing and decreasing steadily.

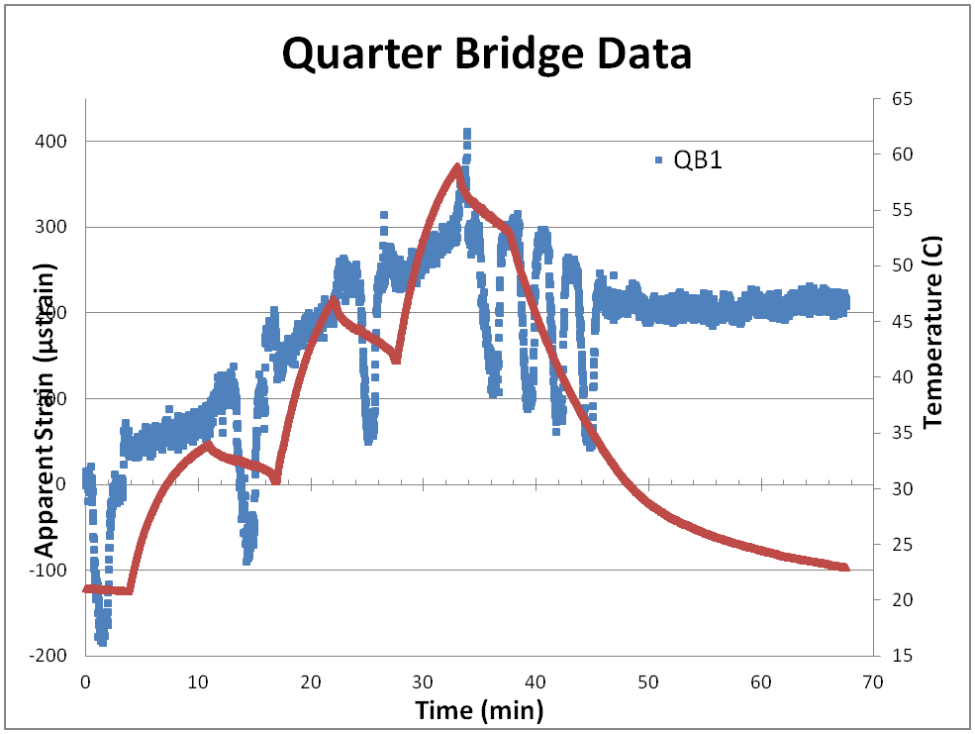

Figure 39: Strain output from quarter bridge MFSG, with temperature (red) showing temperature effects. Each dip in data is when the specimen was removed from the oven and strained. The apparent residual strain after 50 min. is due to drift from resistive heating of the strain gage. This was mediated by using the three-wire strain gages.

Figure 40 represents the half bridge (temperature compensated) strain vs. the quarter bridge strain. It can be seen that temperature effects are completely removed by the half bridge, and only the axial loading events are seen in the half bridge data.

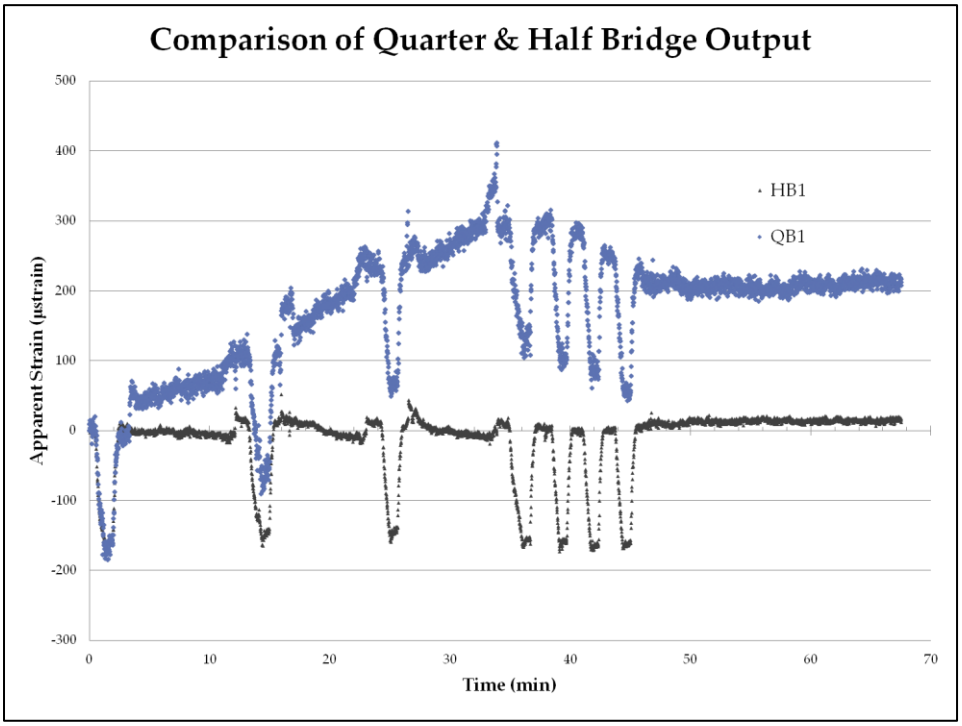

Figure 40: Comparison of Half-Bridge and Quarter-Bridge Strain

Of particular interest from this test was the correlation between the quarter bridge data and temperature. When properly calibrated, strain gages can be used to determine temperature of the composite, without the need for a separate thermocouple and control system. If the half bridge data is subtracted from the quarter bridge data, only temperature effects remain. This could prove especially useful in long-term health monitoring of the composites. This correlation can be seen in figure 41.

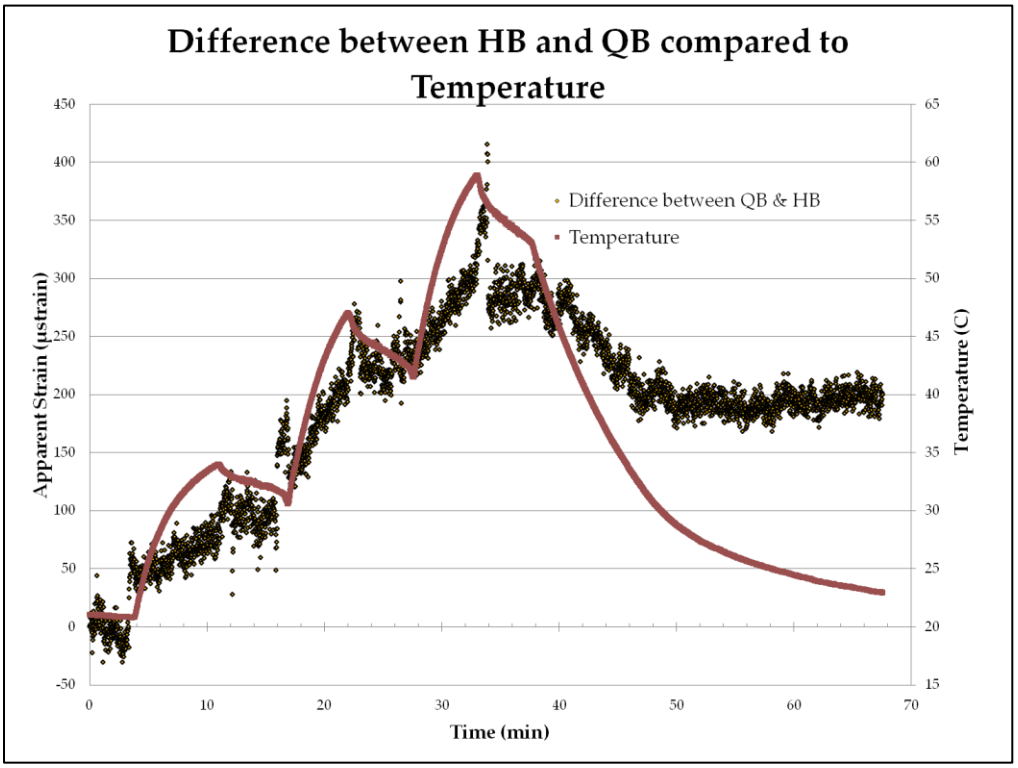

Figure 41: Difference of half-bridge and quarter-bridge strain, showing a good fit of just temperature effects.

Notice that the strain data does not return to zero after the test. This is due to resistive heating of the gages over time. As mentioned previously, this problem was corrected by dropping the Wheatstone bridge voltage from 3V to 1V, and using 3-wire strain gages.

Cure Monitor Results

Once the strain gages and circuits had been tested and verified, the actual cure monitoring of the plates could be performed. The final testing was a progressive process in which many improvements were made to the process, and more accurate results were obtained with each test. The final test, with the master plate, yielded very consistent results, and is considered the benchmark of all of the testing.

The cure monitoring was performed in two steps, room temperature cure, and elevated temperature cure. The room temperature cure process was performed in a composite manufacturing lab with an ambient temperature of about 26 degrees Celsius. The plate laminate was manufactured, and then left on the work bench on which it was manufactured to cure. The elevated temperature cure was performed in an industrial oven.

There were several expected results from these tests. Expected results from the room temperature cure process were to see some induced permanent compressive strain due to the thermochemical shrinkage of the epoxy. This was confirmed in testing. Expected result from the elevated temperature cure was some relaxation of the induced compressive strain, but this expectation was not seen in the final results.

Room Temperature Cure Results

The results from the room temperature testing were as expected, with some compressive strain evident, as a result of the thermochemical shrinkage. Every test, including the early, non-temperature-compensated tests, showed these results. This data is not considered very accurate, as it was not compensated for temperature fluctuations. Every test did, however show compressive trends. This data is included in Appendix B.

Figure 42 shows accurate data from the final master plate testing. The data shown is from a temperature compensated half bridge circuit. It can be seen that the data is independent of the temperature, and just shows a strain component. The initial values that seem erratic are due to the plate injection process. As the resin begins to gel shortly after

injection, the resin begins thermochemical shrinkage, and permanent compressive strain can be seen.

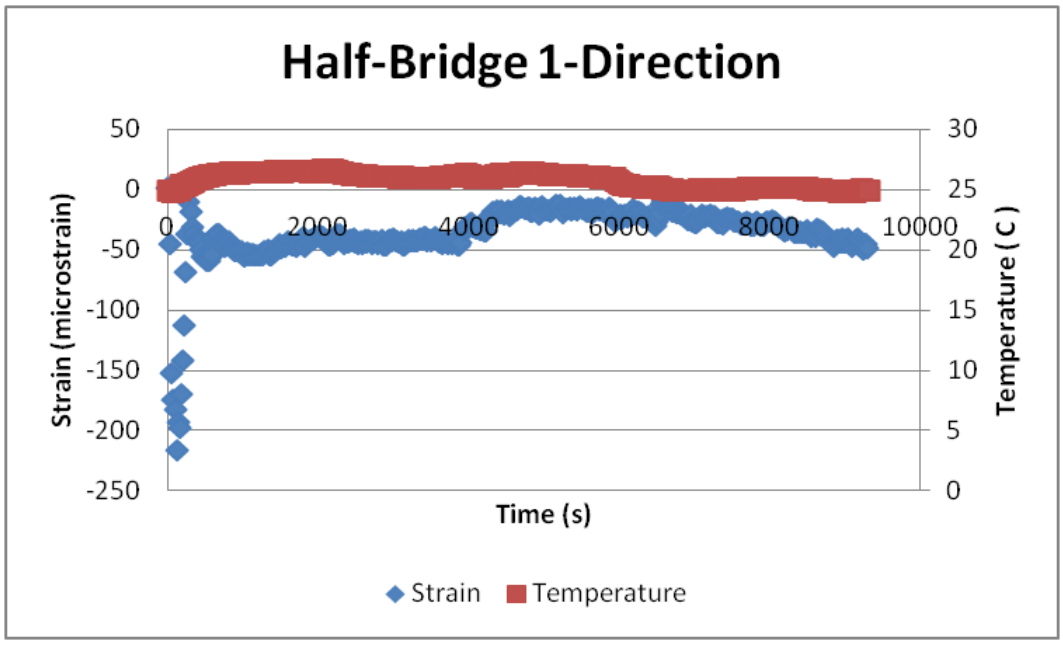

Figure 42: Chart showing permanent compressive strain of approx. 40 microstrain in principal direction from room temperature cure

As can be seen in figure 42, a permanent compressive strain is evident, and can be measured by the embedded strain gages. In this test, a permanent interlaminar compressive strain of 48.5 microstrain in the principal (fiber) direction was measured.

This trend of permanent shrinkage has been confirmed and measured by others with alternate methods. The amount of shrinkage is highly dependent on material type and cure temperature. Some epoxies may shrink by as much as 6% (29), while typical results from others performing similar tests indicate shrinkages of anywhere from 1.5 to 2% (21). Again, shrinkage is highly dependent on material type, cure temperature and

process. In fact, some thermoset polymers have been developed to exhibit near-zero shrinkage, or even slight expansion on cross-linking (30).

Elevated Temperature Cure Results

Once the plate had undergone the 24 hour room temperature cure process, it was placed in an industrial oven to undergo the elevated temperature cure process. It was expected that in this process some relaxation of the permanent compressive strain would occur, similar to annealing, due to relaxation of the resin, but this turned out not to be the case based on the data received, for this resin type. This is evident in figure 43.

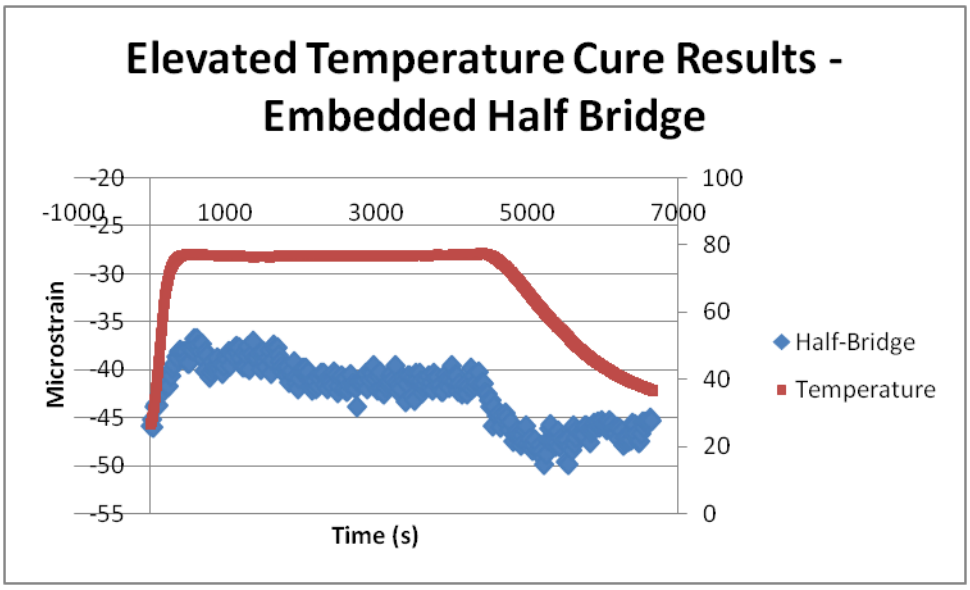

Figure 43: Half bridge strain and temperature (red) in principal direction during elevated temperature cure process. This shows no relaxation of the of the specimen.

From the data in figure 43, it can be seen that the laminate exhibits no relaxation under elevated temperature cure. The physical thermal expansion of the laminate may be

seen in the data, but the permanent compressive strain returns to its original value of approximately 48 microstrain.

It should be noted that these results are typical of the epoxy/fiber combination used here. Some have seen moderate relaxation of the composite upon completion of the elevated temperature cure process, similar to annealing. The compressive strain effects can also be reduced with modified cure temperature profiles (21). The reported relaxation effects seem to be most apparent between laminate layers and are particularly pronounced with thermoplastic resins (20). Even if some annealing occurs during the elevated temperature cure process, there will always be some residual strain due to polymer cross-linking that cannot be removed, as evidenced by the testing done in this research.

Error Analysis

Throughout this testing, due diligence was made in an attempt to reduce error as much as possible. However, as with any scientific process, some amount of error was unavoidable. Sources of error include limitations of the testing equipment, limited sample quantities, and user errors.

Testing Equipment

As was seen in figures 5 and 6 previously, the DAQ used introduced some error based on technical limitations. For the settings used in measurement of MFSG strains, the voltage measurement resolution of the DAQ was calculated to be 0.1 µV. The sensitivity at this measurement range was +/- 5.2 µV. This gives a max error of +/- 10 µstrain based on equipment limitations. For the PVDF measurements, the resolution was calculated at

30.5 µV, with a sensitivity of +/- 68 µV. The typical voltage differentials seen were in the 100-1000 mV range. This gives a maximum error of +/- 0.01% based on equipment limitations. The error in the permanent strain calculations can be seen plotted as error bars in figure 44. The same error applies to the elevated temperature cure data, as can be seen plotted as error bars in figure 45.

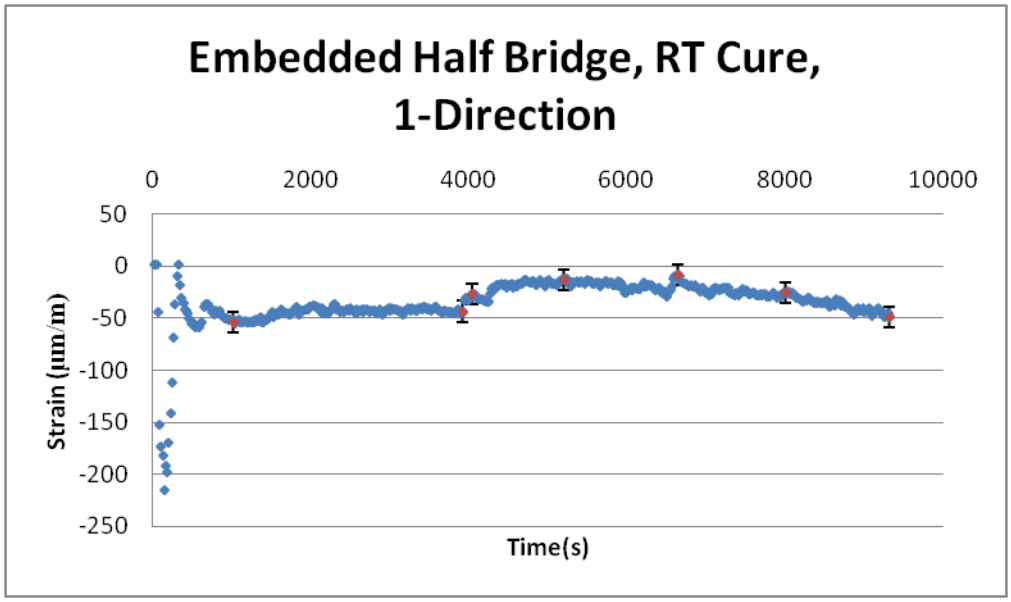

Figure 44: Embedded half bridge data from room temperature cure plotted with error bars.

Limited Sample Quantities

Due to the nature of the laminate samples, they were very expensive and time-consuming to make. Lab space and equipment had to be shared with other researchers, and much analysis was devoted to each plate after manufacture. These factors limited the number of samples that could be manufactured and studied under the reasonable expectations of this work. While the results shown here were shown to be repeatable

through all samples manufactured, ideally a larger sample size would give more statistically significant results.

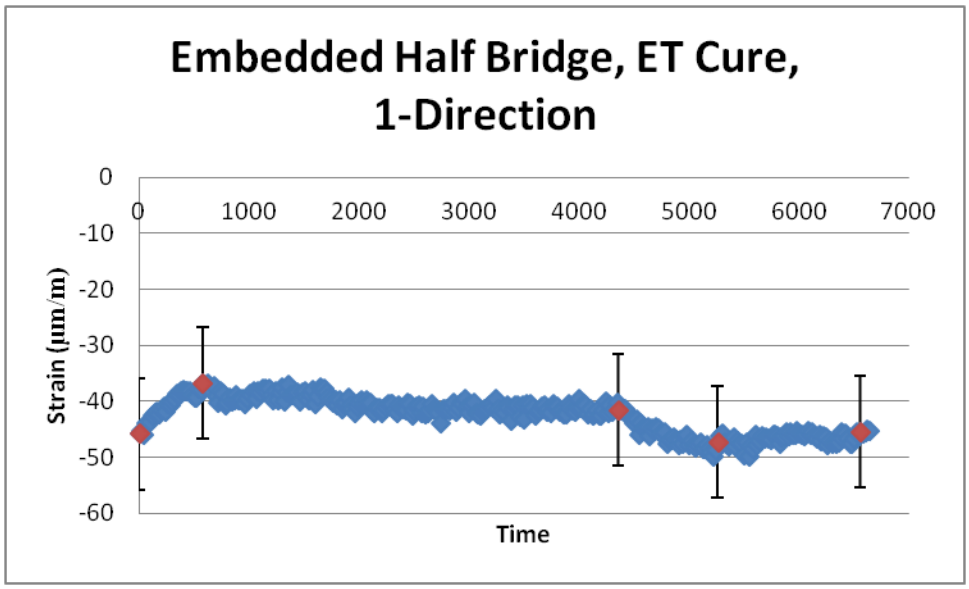

Figure 45: Embedded half bridge data from elevated temperature cure, plotted with error bars.

CONCLUSIONS

Based on the iterative testing process, and the results from the tests performed, some important conclusions may be drawn. These findings can be broken down into three major topics: Sensor Selection, Laminate Construction, and Laminate Curing. These findings are summarized below:

Sensor Selection

- First, in sensor selection, it was determined that although they may be useful in instantaneous testing and load monitoring, the PVDF sensors combined with simple charge amplifier circuits are not feasible for long-term monitoring of stress and strain, or temperature. This is due to the decay within the circuit of the charge produced by the sensor. Modifying the charge amplifier circuit to increase the time constant did not produce a decay long enough to be useful to the testing. Thus, in strictly long-term monitoring situations, PVDF sensors with basic charge amplifier circuits may not effectively be used.
- It was determined that PVDF sensors may be utilized to measure temperature spikes and shock loading situations to good success. This makes them useful for post-cure health monitoring approaches.
- The testing showed that MFSG sensors were the best current solution for measuring cure strains. They rely on simple measurement techniques that may easily be calibrated and temperature compensated.

- MFSG sensors may also be utilized, in the correct configuration, to determine temperature of the sample with no additional sensors or thermocouples required, by analyzing the data from a non-temperature-compensated quarter bridge, and a concurrent temperature-compensated half bridge. This is useful as it reduces circuitry requirements, and the need for additional stocks of sensors.

Laminate Construction

A method for sensor wire extraction from the mold was developed through the course of this research. The method uses a double bag system, in order to cleanly extricate the wires from the mold, while maintaining the mold integrity. After assembling the mold, the wires are taken out through the exterior bag via small slits. Then the wires were fed through a dual layer of Tacky tape that created a small box around the slits. A second bag layer was placed over this small section, and this created a good seal while allowing access to the sensor lead wires.

This process allows for long wires to be used without impeding resin flow, and ensures better mold integrity.

Cure Data

In the initial, room-temperature cure process, it was determined that a residual interlaminar compressive strain of approximately 48 microstrain was seen in the sample, due to thermochemical shrinkage of the epoxy during the cure process. This is an important factor to consider when designing large or critical clearance parts. During the cure process, the shape and size of the parts will change.

During the elevated temperature cure process, it was found that no relaxation of the epoxy occurred, and thus the compressive strain that was induced in the cure process was not relaxed. The sample increased due to thermal expansion, and then relaxed back to its original dimensions upon cooling. Thus the final laminate dimensions are set upon the initial room-temperature cure process for this particular resin/fiber combination. All thermoset polymer resins will indicate some permanent compressive strain, and the sensors may be used to evaluate the degree of this.

RECOMMENDATIONS

PVDF Sensors

PVDF sensors with simple charge amplifier circuits cannot effectively measure long-term events such as cure monitoring. However, PVDF sensors are useful for measuring instantaneous events. Care should be taken when utilizing PVDF sensors to ensure that loading rates are known before analyzing the output in strain situations. PVDF sensors must also be temperature compensated to give useful strain results.

MFSG Sensors

MFSGs gave consistent results during cure monitoring and post-cure health monitoring. For most cure monitoring applications, they must be temperature compensated in order to account for thermal strains. This is done through the use of a combination of half and quarter Wheatstone bridges. Also, three-wire strain gages should be used to obtain more accurate long-term results.

Cure Monitor

The double-bagging method outlined here should be used for sensor wire access to the mold for cure monitoring purposes. This enables better resin flow and ensures mold integrity, while allowing for good access to the wires, and keeping them from being encased in resin.

FUTURE WORK

Montana State University is currently involved in ongoing work with composite manufacturing research for wind turbine and hydrokinetic blades. This work will aid future composite laminate research. The cure monitoring results presented here should be tested and validated on full-scale laminate layups of wind turbine blades.

PVDF Sensor Work

One of the main areas of this research that warrants further work is PVDF sensor use. PVDF sensors are very sensitive, accurate sensors when used in the proper context. While they did not work for long-term monitoring in the configuration presented here, they show much promise for use as health monitors and shock and failure indicators in installed laminates. It is also possible that the various charge/decay trends indicated by these sensors may be analyzed and quantized to give useful steady-state results as well. This may also be accomplished by analyzing the data spikes they produce. This was outside the scope of this research. This work showed that they are not capable of producing useful long-term steady-state results in simple strain monitoring situations, but they should continue to be investigated for use as sensors within the realm of composite research.

Fiber Optic Sensor Work

Much work is being performed in many programs across the world with fiber optic strain sensing. This is a very promising approach to laminate strain monitoring. It would be possible to develop a single fiber that ran the length of a wind turbine blade,

that could give strain results for each portion along the blade. Additionally, it is possible that in manufacturing the fiber mats, these sensors could be inserted along with the regular fibers, essentially creating no defects in the part. Many of the fibers could be inserted, creating a grid with which the entire blade could be monitored in two and three dimensions. More research into fiber optic strain sensing would be a great benefit to composite design and development.

Cure Monitoring

This research acts as a baseline for establishing methods for cure strain monitoring. Much work remains to be done in the field of using embedded sensors for cure monitoring. In thick composite laminates, significant variances in through-thickness properties can be observed. Of interest would be to measure the various interlaminar stresses between each ply. Also, in thick, complex geometries, with ply drops, or other geometric anamolies, the difference in strain seen in the layers around that area would be of interest.

Health Monitoring

Once the sensors are used in initial cure monitoring, they must necessarily remain embedded within the laminate. This means that, if properly placed and developed, they can be used for future monitoring of the laminates to measure loading, and test for integrity of the part. This aspect of the laminate monitoring was explored by Meehan in his thesis work, using the laminates developed in the process of this research. This area

could be further explored, creating laminates with sensors placed in specific locations, and with specific orientations, to monitor critical areas of the finished part.

With all of the research currently being performed in smart materials (materials that may significantly alter their properties via external stimulus), more research should be channeled into developing and refining smart composites. The possibilities of what can be created upon the merging of composites technology with smart materials technology are astounding.

Composite materials continue to be a rapidly growing alternative to traditional engineering materials. This trend looks to continue for the foreseeable future. Thus, every effort must be made to continue to understand and refine composite materials, and manufacturing methods, in order to produce products that enable life in an ever challenging environment.

-Jason Mills, 2013

REFERENCES CITED

Bibliography

1. *"Water Mills in the Area of Sagalassos: A Disappearing Ancient Technology".* **Donners, K., Waelkens, M. and Deckers, J.** 2002, Anatolian Studies, Vol. 52, pp. 1-17.

2. *Heron's Windmill.* **Drachmann, A.G.** 1961, Centaurus, pp. 145-151.

3. *James Blyth - Britain's first modern wind power engineer.* **Price, Trevor J.** 2005, Wind Engineering, pp. 191-200.

4. **Wind Power, Monthly.** The 10 Biggest Turbines in the World. *www.windpowermonthly.com.* June 2013.

5. **Greg Wetstone.** *Terra-Gen Power Announces Closing of $650 Million Construction Financing for Alta Wind VII & IX to Continue Build-Out of Nation's Largest Wind Energy Facility.* New York : Terra-Gen Power, LLC, 2012.

6. **Invenergy, LLC.** *Judith Gap Wind Farm.* s.l. : Montana DNRC, http://dnrc.mt.gov/Trust/Wind/JudithGap.asp, 2005.

7. **Scott, I.G. and Scala, C.M.** *A Review of Non-Destructive Testing of Composite Materials.* s.l. : NDT International, 1982.

8. **Barbero, Ever J.** *Introduction to Composite Materials Design, 2nd. Ed.* Boca Raton : CRC Press, 2011.

9. **Hon, David and Shiraishi, Nobuo.** *Wood and Cellulose Chemistry, 2nd ed.* New York : Marcel Dekker, 2001.

10. **Palmer, Nathan R.** *Smart Composites: Evaluation of Embedded Sensors in Composite Materials.* Bozeman : Montana State University, 2009.

11. **Ehresman, Jon.** *Integration of Actuators and Sensors into Composite Structures.* Bozeman : Montana State University, 2009.

12. **Blockey, J.C.** *Feasibility in Developing Smart Structures for Use in Wind Turbine Blades.* Bozeman : Montana State University, 2008.

13. *An embedded FBG sensor for simultaneous measurement of stress and temperature.* **Gin, L. and Kai, G.** 2006, IEEE Photonics Technology Letters, pp. 154-156.

14. *Photosensitivity in optical fiber waveguides: application to reflection fiber fabrication.* **Hill, K.O., et al.** 1978, Applied Physics Letters, p. 647.

15. *Fiber Optic Sensors for Cure/Health Monitoring of Composite Materials.* **Wood, K.H.** 2004, NASA Technical Documents.

16. *Real-time cure monitoring of smart composite materials using extrinsic Fabry-Perot interferometer and fiber Bragg grating sensors.* **Leng, JS and Asundi, A.** s.l. : Smart Materials and Structures, 2002, Smart Materials and Structures, p. 249.

17. *Cure monitoring of composite laminates using fiber optic sensors.* **Kang, Hyun-Kyu et. al.** 2002, Smart Materials and Structures, p. 279.

18. **Kang, HK.** *Development of Fiber Optic Ingress/Egress Methods For Smart Composite Structures.* s.l. : Korea Advanced Institute of Science and Technology, 2000.

19. **Udd, et. al.** *Failure Mechanisms of Fiber Optic Sensors Placed in Composite Materials.* 2005.

20. **Parlevliet, Patricia.** *Residual Strains in Thick Thermoplastic Composites.* s.l. : Technische Universiteit Delft, 2010.

21. *In Situ Monitoring of Residual Strain Development During Composite Cure.* **Crasto, Allan, Kim, Ran and Russell, John.** 2002, Polymer Composites.

22. **Gautschi, Gustav H.** *Piezoelectric Sensorics.* s.l. : Springer, 2006.

23. **Omega.** *Thermocouple - An Introduction.* s.l. : www.omega.com, 2012.

24. **Vishay Precision Group.** *The Three-Wire Quarter Bridge Circuit.* s.l. : Micro-Measurements.com, 2010.

25. **Weber, Manfred.** *Application Note - Piezoelectric Accelerometers.* s.l. : MMF.

26. **Webster, John G.** *The Measurement, Instrumentation, and Sensors Handbook.* s.l. : CRC Press, 1999.

27. **Beukema, RP.** *Embedding Technologies of FBG Sensors in Composites: Technologies, Applications and Practical Use.* s.l. : 6th European Workshop on Structural Health Monitoring - Tu.4.C.4, 2012.

28. **Steven Gordin, Akbar M. Eslami, Howard L. Price.** *Gel Time and Temperature for Two Thermosetting Resins.* s.l. : American Society for Engineering Education, 2004.

29. **Yates, B and Al., Et.** 1979, Journal of Materials Science, p. 14.

30. *Physical and mechanical characterization of near-zero shrinkage polybenzoxazines.* **Ishida, Hatsuo and Allen, Douglas.** 1996, Journal of Polymer Science, pp. 1019-1030.

31. **Lockhart, Roger.** *How Much ADC Resolution Do You Really Need?* s.l. : DATAQ, http://www.dataq.com/applicat/articles/adc-resolution.html, 2013.

APPENDICES

APPENDIX A

SENSOR TESTING MATRIX

Test	# of Speci-mens	# of Tests/ Specimen	Specimen Geometry	Loading Configuration	Reason for Test	Parameter being measured	Results/Notes
12-hour steady-state sensor output	2	2	Mid-plane of full plate.	No loading, steady state.	To determine noise threshold/test circuit modifications	Output voltage of half and quarter Wheatstone bridges and charge amplifier circuits (mVDC)	Circuit/DAQ improvements were made until noise was reduced to +/- 1% of steady-state value
Heating tests of half-bridge and quarter-bridge MFSG samples	2 ea.	3	Mid-plane of sectioned plate samples, 5x10cm.	Sectioned samples placed in small industrial oven.	To determine whether temperature could be removed from response by utilizing a dummy sample in a half bridge setup.	Output of half and quarter Wheatstone bridges (mVDC)	See Figs. 36-38. Temperature was successfully separated from results, until resistive heating skewed end results (note that this problem was resolved by dropping supply voltage from 3 V to 1V, and using three wire strain gages.)

Heating test of PVDF sensors (bare sensors)	1	1	PVDF Sensor	Sensor placed in small industrial oven.	To determine temperature response of PVDF	Charge amplifier circuit voltage (mVDC)	PVDF film would flap in wind created by convection oven. This skewed results
Heating test of PVDF sensor adhered to aluminum bar	1	2	PVDF Sensor adhered to 6061-T6 aluminum bar stock, 3x2x10cm.	Sensor and bar placed in small industrial oven.	To determine temperature response of PVDF	Charge amplifier circuit voltage (mVDC)	Due to charge decay, a good representation of temperature was not possible. This was partly due to the minor temperature changes as the convection oven attempted to maintain constant temperature
Heating test of PVDF sensor attached to large aluminum heat sink	1	2	PVDF Sensor adhered to aluminum bar stock in previous test, covered by block of 6061-T6 aluminum, 6x6x10cm.	Sensor bar and heat sink assembly placed in small industrial oven.	To determine temperature response of PVDF	Charge amplifier circuit voltage (mVDC)	In an attempt to reduce temperature fluctuation seen by sensor, a large block of aluminum was utilized as heat storage. Because the CTE of the aluminum was known, PVDF could be characterized. However, given that PVDF films are not appropriate in long-term monitoring situations, this gave no useful results.

Bending test of PVDF sensor.	1	2	PVDF sensor adhered to thin steel bar, 0.2x2x25cm.	Cantilever beam loading with a weight attached to free end.	To determine long-term response of PVDF to mechanical strain	Charge amplifier circuit voltage (mVDC)	In order to test the long-term response of the PVDF in long-term strain, the PVDF was mounted to a thin steel bar that was loaded in bending. The PVDF sensor accurately portrayed the strain, but when the bar was held in its strained position, would return to zero due to charge decay. (see Figs. 30 and 31)
Axial strain test of laminate sample with both MFSG and PVDF sensors.	2	2	PVDF and MFSG sensors adhered to aluminum bar, 0.3x2.5x15 cm.	Instron tensile tester, specimen clamped on ends with jaws.	To determine the response of PVDF sensor in axial loading conditions.	Charge amplifier circuit voltage (mVDC)	As can be seen in Fig. 32, a sample with both an MFSG and a PVDF sensor was loaded at a constant stress rate of 66 N/s to determine the response, and compare the response. At a loading of approx. 850 microstrain, the test was paused and allowed to rest. It can be seen that, while the MFSG remained at SS, the

							PVDF returned to zero, and then showed compressive strain as it was unloaded.
Axial Loading of Specimen Under Various Loading Rates	1	5	PVDF sensor adhered to aluminum bar 0.3x2.5x15 cm.	Instron tensile tester, specimen clamped on ends with jaws.	To determine the effect of various loading rates on sensor output	Charge amplifier circuit voltage (mVDC)	Loading rate appears to significantly affect PVDF output from strain loading. The values varied between each sample for maximum value reached, and area under loading curve (comparable to charge density).
PVDF loading with different time constants in charge amplifier	1	3	PVDF sensor adhered to aluminum bar 0.3x2.5x15 cm.	Instron tensile tester, specimen clamped on ends with tester jaws.	To determine the effect of changing charge amplifier time constant on loading response.	Charge amplifier circuit voltage (mVDC)	Several different time constants were tried to see if the decay could be extended long enough to obtain useable long-term strain results from the PVDFs. However, the results were so minimal as to not be applicable.

APPENDIX B

ADC RESOLUTION

In order to determine the ADC (analog to digital converter) resolution of the data acquisition hardware used, the National Instruments data sheets were consulted. The bit rate was determined, and the following equation 6 (31) for determining resolution was applied.

$$R = \frac{V_D}{V_S \times 2^{(n-B)}} \times E$$

Equation 6: Equation for determining DAQ resolution based on bit rate.

Here R is the resolution, V_D is the full scale range of voltage measurement, V_S is the source voltage being measured. "n" is the bit rate of the ADC, and B is a value given for whether the ADC is polar or bipolar. E is the full scale of the physical quantity being measured, in this case, also voltage.

Using the following values, in addition to the values found in table 7, the values given for resolution in table 8 were determined.

Table 10: DAQ Values for determining resolution

Parameter	Value
Bit rate, n	16
Polar/Bipolar	Bipolar, 1

APPENDIX C

RAW DATA PLOTS

Raw Data from testing, prior to any processing.

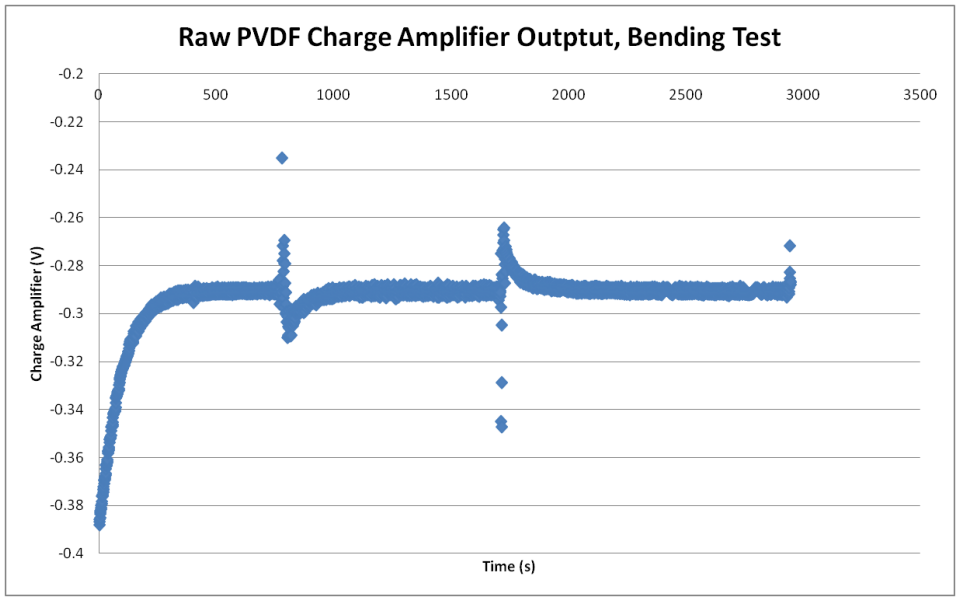

Figure C1: Raw data from PVDF bending test. The chart shows charge amplifier output voltage.

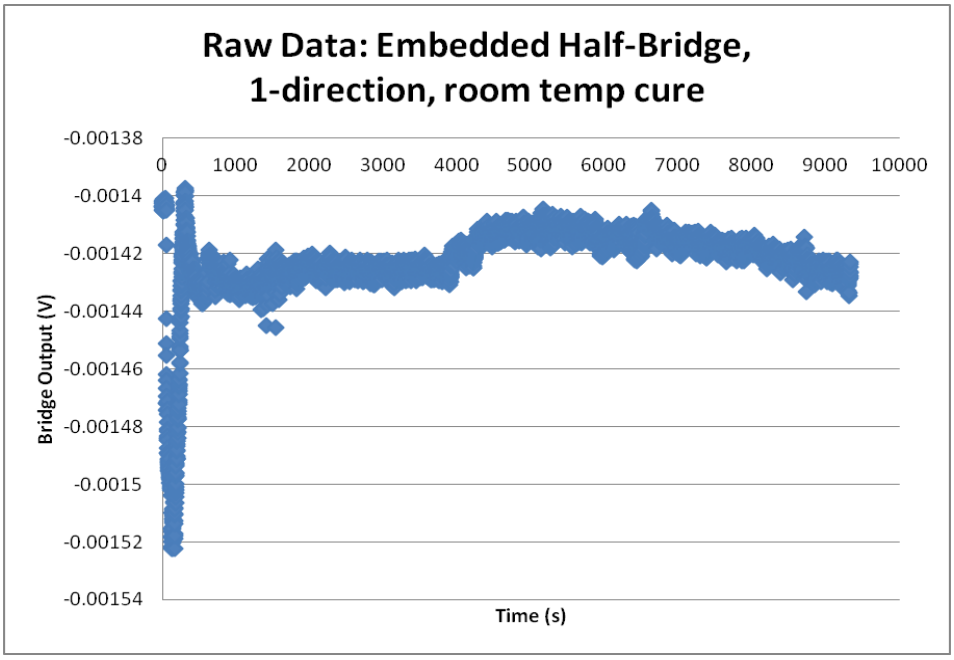

Figure C2: Raw data from embedded half-bridge MFSG, oriented in 1-direction. From final “master” plate, room temperature cure.

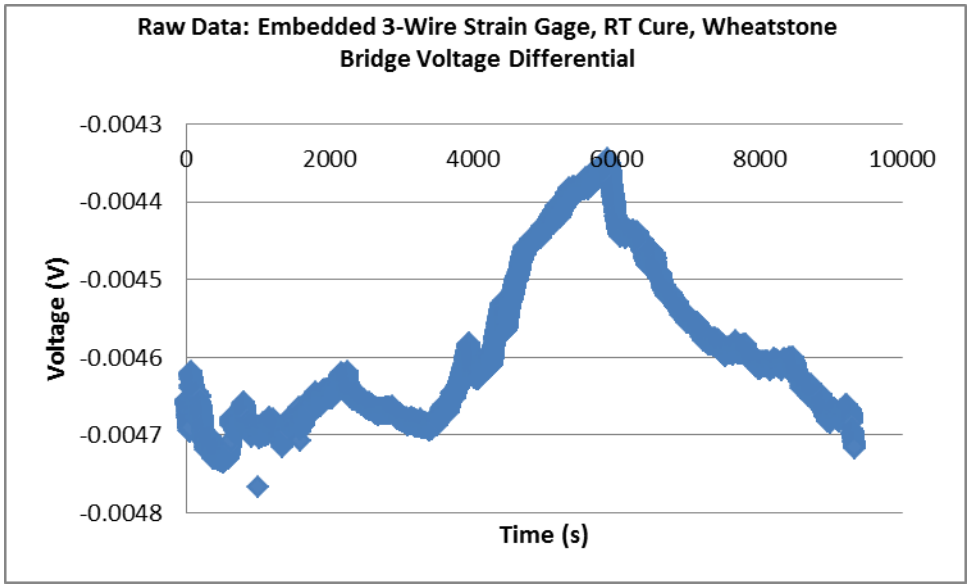

Figure C3: Raw data from embedded 3-wire strain gage, 1-direction, room temperature cure. This is from the final "master" plate. Voltage is difference across Wheatstone bridge.

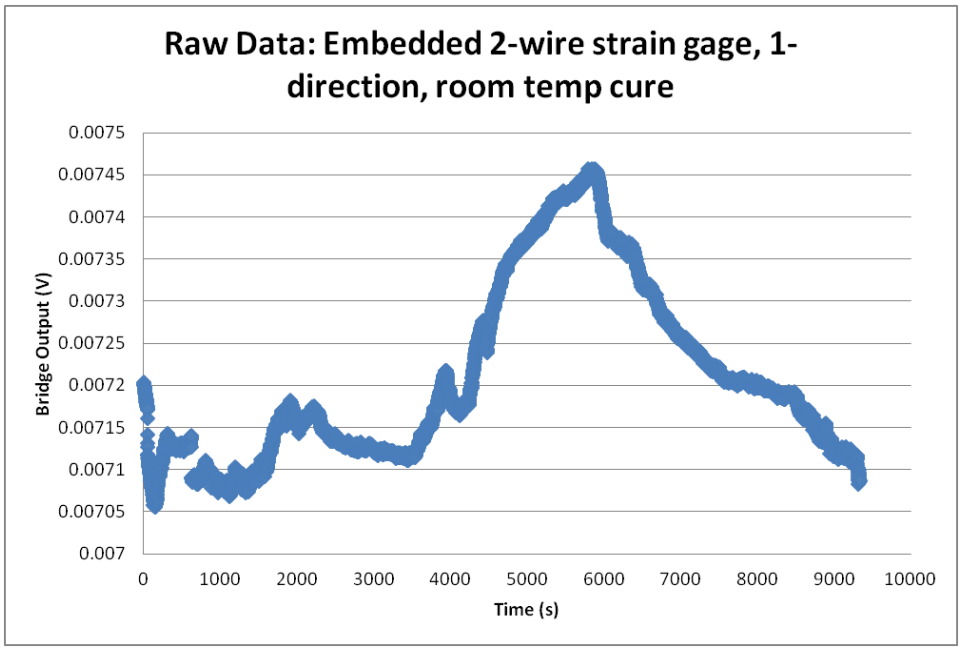

Figure C4: Raw data from embedded 2-wire strain gage, oriented in 1-direction. From room-temp cure, final master plate. Output is Wheatstone bridge differential.

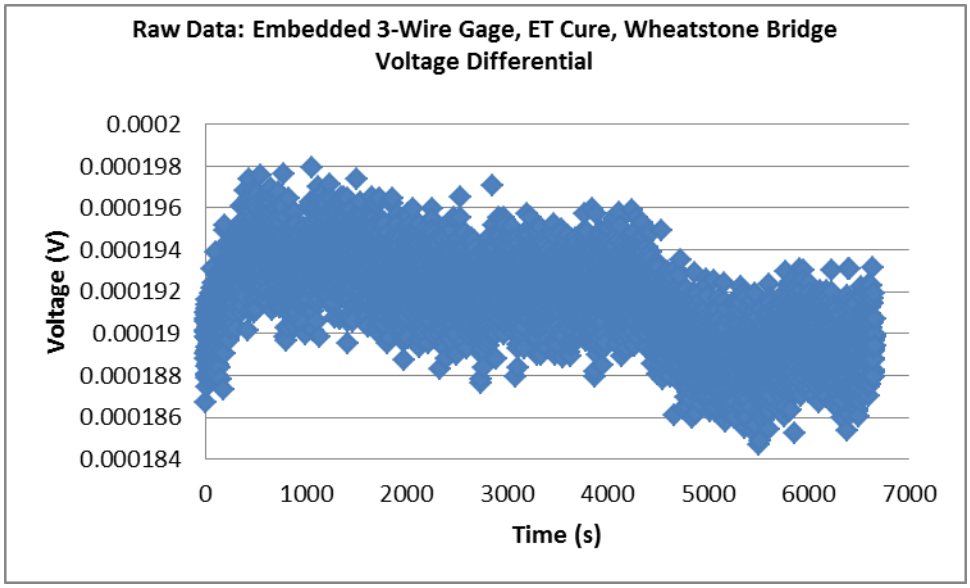

Figure C5: Raw data from embedded 3-wire strain gage, 1-direction, elevated temperature cure. This is from the final "master" plate. Voltage is difference across Wheatstone bridge.

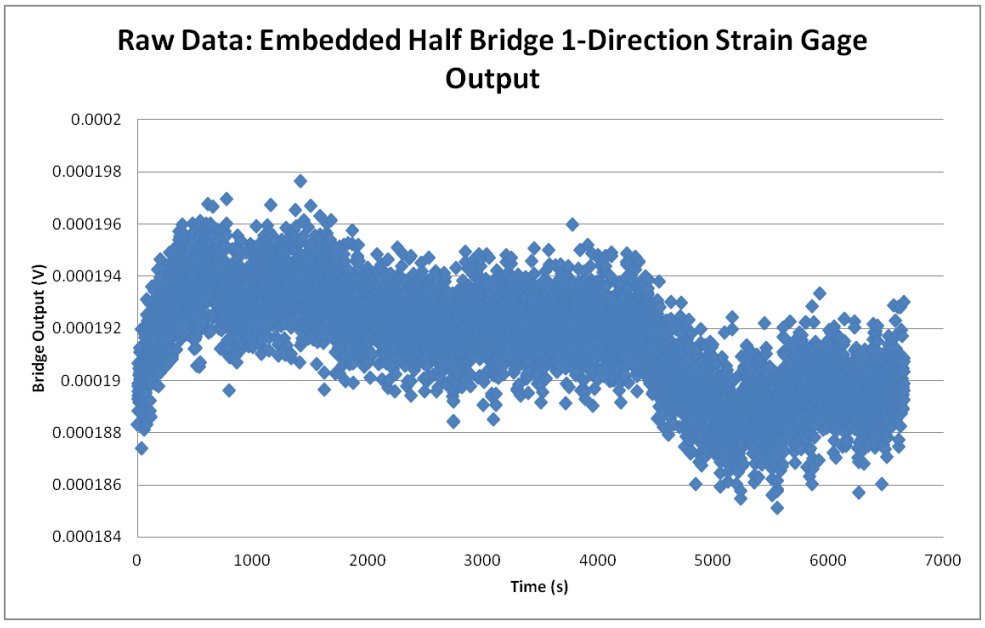

Figure C6: Raw data from embedded half bridge oriented in 1-direction, elevated temperature cure. This is from the final "master" plate. Voltage is difference across Wheatstone bridge

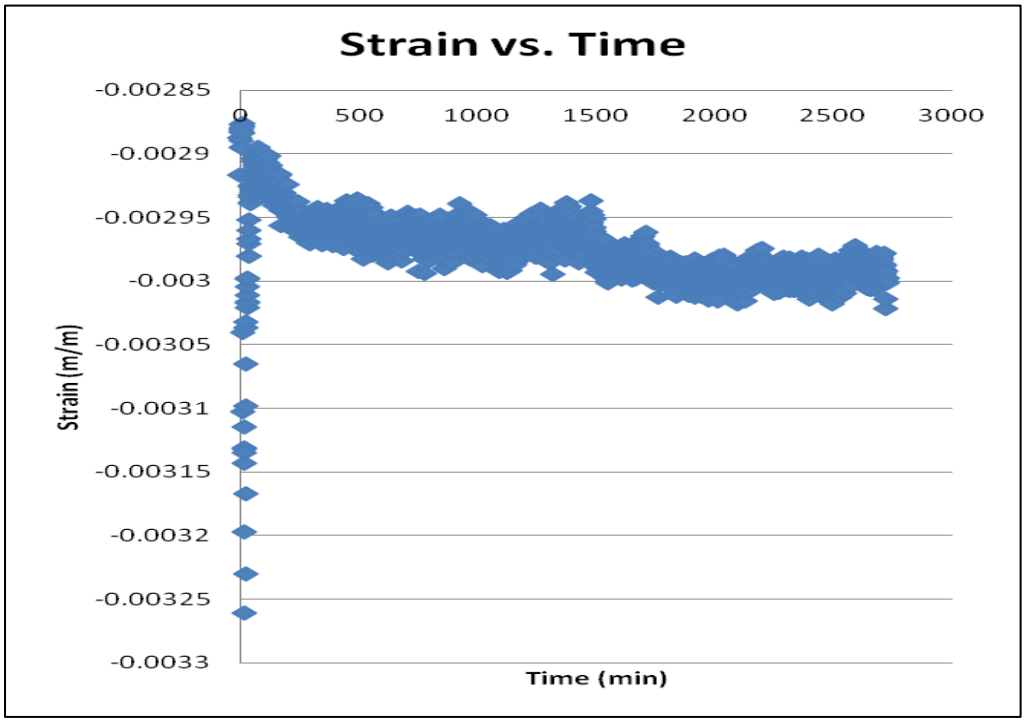

Figure C7: Data from early plate test showing trend toward permanent compressive strain